ABSTRACT

KISEOK JANG. Understanding the UV Reactor Performance: A Lagrangian viewpoint. (Under the direction of Dr.Joel Ducoste.)

The UV dose distribution has long since been the primary source of information that completely describes the performance of a UV reactor for a single operating and or water quality condition. Currently, there are only two approaches to determine the dose distribution: 1) Fluorescent microspheres and 2) Computational fluid dynamics (CFD). Fluorescent microspheres have recently become an approach to validate the CFD predicted dose distribution. Unlike CFD modeling, however, they cannot reveal the UV intensity field or residence time distribution (RTD) that is needed for improved understanding of the behavior inside the UV reactor. In this research, RTD, UV intensity distribution and the relationship between them have been investigated by using modeling data from four different UV reactors under multiple operating conditions. This data was then evaluated as a possible alternative method for analysis of UV reactors. Additionally, the coefficient of variation (CV) for residence time and UV intensity were calculated using the UV modeling data for further understanding of the UV reactor performance. In some cases, analysis indicated that reactor configurations with very similar UV dose distribution had substantially different UV intensity distributions and RTDs, indicating a possible alternative analysis technique for UV reactors that could provide greater insight into the internal workings of the system. An experimental procedure using a wireless UV detector was introduced to measure residence time and UV intensity in the pilot test. Although there were still several limitations of the UV detector to accurately measure the UV intensity field from the point of view of the microorganism, the device displays potential to measure the local residence time and UV intensity.

Understanding the UV Reactor Performance: A Lagrangian viewpoint

by
Kiseok Jang

A thesis submitted to the Graduate Faculty of
North Carolina State University
in partial fulfillment of the
requirements for the Degree of
Master of Science

Civil Engineering

Raleigh, North Carolina

2008

APPROVED BY:

_____	_____
Dr. Detlef R.U. Knappe	Dr. Francis de los Reyes

_____
Dr. Joel Ducoste
Chair of Advisory Committee

BIOGRAPHY

Kiseok Jang was born on January 30th, 1979 in Daegu, South Korea. He is second child of Mansu Jang and Chuna An. He spent 18 years in Daegu until he finished her high school there. He graduated from Korean Military Academy in March 2001 with a bachelor's degree in Civil Engineering. After serving in construction area for 4 years, he came to the United States in August 2006 to pursue his Master of Science in Environmental Engineering with Department of Civil, Construction and Environmental Engineering at North Carolina State University. After graduate from North Carolina State University, he will return to South Korea expecting to be involved in environmental work.

TABLE OF CONTENTS

LIST OF TABLES

LIST OF FIGURES

Introduction

UV disinfection for drinking water is quickly becoming a significant process because it currently does not produce any known inactivation by-products. In addition, UV light has been effective at the inactivation of some chlorine-resistant pathogens, such as Cryptosporidium and Giardia (USEPA).

Because UV disinfection is considered one of the alternatives to chemical disinfectants, a number of research studies have been performed to characterize the UV reactor behavior by measuring the emitted UV dose.

USEPA recommends using biodosimetry as a validation protocol to measure the UV dose. The log inactivation of a microorganism is measured from full-scale reactor test under specific operating conditions including flow rate, UV transmittance (UVT), and UV intensity. The log inactivation value is input into the dose-response equation obtained from the bench scale test to produce the Reduction Equivalent Dose (RED). The validation dose can then be calculated by dividing RED by the validation factors (VF), which result from the hydraulic effects of the installation and the UV reactor equipment (USEPA, 2006). Due to these factors, the Long Term 2 Enhanced Surface Water Treatment Rule (LT2ESWTR), which considers UV disinfection as one of the alternative treatments for reducing microbial contamination of drinking water, requires UV reactors to be validated for application in public water systems (PWSs). However, a validation dose obtained from biodosimetry at a validation facility is not enough to explain UV

reactor performance due to fluid velocity variations in reactors. In continuous flow systems, there is not an average dose but instead a dose distribution due to the broad range of fluid element travel paths and variations in the UV intensity (Cabaj et al., 1996; Lin and Blatchley, 2001; Unluturk and Arastoopour, 2004; Bohrerova et al., 2005).

Recently, one alternative approach to biodosimetry for UV reactor validation is the use of microspheres that undergo a chemical reaction when UV light is irradiated. UV dose distribution can be obtained using microspheres released upstream from the UV reactor that are collected and analyzed in the effluent. Fluorescent microsphere can explain the characterization of UV reactor better than the average UV dose obtained experimentally with biodosimetry and can be used for reactor validation or optimization as a result of direct measure of UV dose distribution in a reactor (Anderson and Zhang, 2003). The fluorescent microspheres technique serves as a complement to the biodosimetry test by providing better analysis of reactor behavior (Bohrerova et al., 2005; Blatchley et al., 2008) and can validate the UV dose distribution predicted by mathematical models to improve confidence in the use of models (Bohrerova et al., 2005; Zhao, 2007).

Along with the development of these experimental methods to verify the performance of the UV reactor, computational fluid dynamics (CFD) was introduced to predict microbial movement and inactivation through a UV reactor. UV reactor performance modeling by Eulerian and Lagrangian methods are investigated where the position of microorganisms in the reactor is tracked by the Eulerian or Lagrangian reference frames and the absorbed dose at each point is calculated by multiplying time by the average local fluence rate

(Janex et al., 1998; Lyn and Blatchley, 2005; Ducoste et al., 2005; Sozzi and Fariborz 2006).

With this data, various UV dose distribution curves may be obtained to show specific characterization of each reactor. However, microspheres cannot reveal the UV intensity field or RTD. Qualls and Johnson (1983) concluded that it is essential to determine the UV intensity distribution and RTD to better evaluate the relationship between actual disinfection in flow-through systems and batch experiment results. True understanding of the behavior inside the reactor requires knowledge of the RTD and UV intensity distribution.

Until now, no study has been performed to characterize the individual microbial residence time and expected UV intensity to better understand the dose delivered by the UV reactor. Based on the approach used to develop the dose distribution, the same UV dose may be obtained when microorganisms have either longer residence times with low UV intensity or shorter residence times with higher UV intensity (Unluturk and Arastoopour, 2004). In other words, a single UV dose could result from different combinations of residence time and UV intensity. Consequently, a better understanding of the reactor performance could be obtained by separately analyzing the residence time distribution and UV intensity distribution.

In this study, the UV intensity distribution and RTD from several modeling data were analyzed to determine if both distributions can provide more detailed information about

the UV reactor's performance compared with its current analysis methods using UV dose distribution. To verify the results of residence times and UV intensities from modeling data, an electronic Lagrangian UV sensor designed to measure UV intensity at small time increments was developed and tested on a low-pressure, high-output reactor.

Materials and Methods

Modeling data analysis

Data from CFD models of four different UV reactor designs with several operating conditions were used in this study. TABLE 1 displays the operating conditions for the UV reactors shown in Figure 1. CFD models utilized a Lagrangian Particle Tracking technique that simulates the movement of about 1500 microorganisms through the UV reactor. Using a FORTRAN program, information about 1500 microorganisms that have residence times and average UV intensities for each microorganism were obtained and saved on an Excel spreadsheet (Equation 1). The UV dose received by each microorganism was calculated by integrating the UV intensity over a time interval using Equation 2.

$$I_{avg,j} = \frac{\sum_{1}^{i} I_{i,j} \times \Delta t}{t_j} \quad (1)$$

$I_{avg,j}$: Average UV intensity for j_{th} microorganism
$I_{i,j}$: i_{th} UV intensity measured from j_{th} microorganism simulation
t_j : Residence time for j_{th} microorganism
Δt : Time interval for one UV intensity measure

$$D_{avg,j} = \sum_{1}^{i} I_{i,j} \times \Delta t_j \quad (2)$$

$D_{avg,j}$: Average UV dose for j_{th} microorganism

1. Computation of Residence time distribution (RTD) and UV intensity distribution

In the ideal plug flow reactor (PFR), all microorganisms have the same residence time because of the "no dispersion" assumption in the axial direction of flow in the reactor. The variance of the residence time is zero in a PFR. By comparing variances obtained from different reactor configurations under several conditions, an analysis can be done to compare how closely certain UV reactors behave like an ideal PFR. The residence time coefficient of variation (CV_t) was used in this study to provide additional information to compare the different reactors in TABLE 1, which have different average residence times. CV_t distribution plots were made by calculating CV_t for each microorganism (Equation 3). These distribution plots show the fraction of microorganisms that have a certain CV_t based on the average residence time for a reactor. The CV_t for each reactor was calculated by averaging CV_t for each microorganism (Equation 4).

$$CV_{t,j} = \frac{\sqrt{(t_{avg} - t_j)^2}}{t_{avg}} \tag{3}$$

$CV_{t,j}$: Residence time coefficient of variation for j_{th} microorganism
t_{avg}: Average residence time for a reactor
t_j : Residence time for j_{th} microorganism

$$CV_{t,reactor} = \frac{\sum\sqrt{(t_{avg} - t_j)^2}}{t_{avg} \times N} \tag{4}$$

N: The number of microorganisms for each reactor

According to the Beer-Lambet law, light absorbance for liquid is defined as product of the absorption coefficient of the substance and path length (i.e. light absorbed by microorganisms is non-linear with respect to the path length in the UV reactor). Accordingly, UV light in reactors is not a mixed quantity and the amount of light absorbed by microorganisms depends on position of microbes in UV reactors. In the ideal PFR, all microorganisms have the same average UV intensity in terms of an individual microorganism because the fluid is perfectly mixed in the radial direction of the UV lamp within the reactor, but not in the axial direction of the lamp. Therefore, for the ideal PFR, the variance of UV intensity exposed by all microorganisms in the reactor is zero. By comparing the variance for different reactor cases under several conditions, one can see how closely certain reactors operated to ideal PFR. Because every case has separate average UV intensity in terms of the reactor, a comparison of the coefficients of variation is needed in lieu of variance. Like analysis of residence time, CV_I for each microorganism was calculated and used for making CV_I distribution plots (Equation 5). CV_I for each reactor was calculated by averaging CV_I for each microorganism (Equation 6).

$$CV_{I,j} = \frac{\sqrt{(I_{avg} - I_j)^2}}{I_{avg}} \tag{5}$$

$CV_{t,j}$: UV intensity coefficient of variation for j_{th} microorganism
I_{avg}: Average UV intensity for a reactor
I_j : Average UV intensity for j_{th} microorganism

$$CV_{I,reactor} = \frac{\sum\sqrt{(I_{avg} - I_j)^2}}{I_{avg} \times N} \tag{6}$$

N: The number of microorganisms for each reactor

From the UV intensity data for individual microorganisms, average UV intensity for a reactor and the fraction of microorganisms exposed to a higher than average UV intensity during travel through the reactor were calculated and compared for different reactors with several different operating conditions.

The UV intensity is strongly related to the position of the microorganisms within the irradiated zone of the UV system so that the UV intensity exposed to the microorganisms will increase rapidly as the microorganisms move closer to the lamp. The fraction of microorganisms exposed to higher UV intensities indicates how many microorganisms travel comparatively close to the lamps within the reactor. Since microorganisms with a higher than average UV intensity are more likely to be exposed to higher UV intensity during travel through the reactor, it could be said that those microorganisms take more efficient inactivation paths. In other words, it can be said that reactors with a higher fraction of microorganisms with higher intensity are more efficient in terms of the reactor's performance. Design modifications that produce these paths could potentially allow designers to reduce the lamp power and still achieve the target average UV dose with the new UV reactor design.

As discussed earlier, a certain UV dose could result from either the combination of a long residence time and low intensity or the combination of a short residence time and high intensity. Accordingly, separate analysis of the residence times and UV intensity is needed for better understanding UV reactor performance so that other tools for deciding efficiency of the reactor performance can be developed. Contour plots were developed in

Excel with normalized residence times on the x-axis and normalized UV intensities on the y-axis to display the fraction of microorganisms with certain combinations of residence time and average UV intensity. Normalized residence times and normalized UV intensities were calculated by dividing residence time for a microorganism and UV intensity for a microorganism by average residence time and average UV intensity for a reactor, respectively.

$$\text{Normalized Residence time} = \frac{\text{Residence time for a Particle}}{\text{Average Residence time}} \tag{7}$$

$$\text{Normalized UV intensity} = \frac{\text{UV intensity for a Particle}}{\text{Average UV intensity}} \tag{8}$$

On the contour plot, normalized residence time was divided into nine areas with an interval of 0.1*average residence time on the x-axis. Normalized UV intensity was also divided into nine areas with an interval of 0.2*average UV intensity in the y-axis (Figure 2).

In the contour plot (Figure 2), all microorganisms passing through the reactor can be divided roughly into four quadrants each having representative combinations of residence time and average UV intensity, such as short residence time and low UV intensity; short residence time and high UV intensity; long residence time and low UV intensity; and long residence time and high UV intensity. The upper left quadrant on the contour plot indicates the fraction of microorganisms having relatively short residence time and low UV intensity during travel through the reactor (Figure 2). Conversely, the lower right

quadrant on the contour plot displays the fraction of microorganisms that traveled through the reactor with a relatively long residence time and high UV intensity. The four quadrants can basically represent general regions that microorganisms take within the reactor. When a microorganism takes a path close to the lamps and passes through a reactor with a faster than average residence time, that microorganism has a relatively short residence time and high average UV intensity based on average residence time and average UV intensity, which is found in the lower left quadrant of the contour plot. If a microorganism takes the path closer to the reactor wall and passes slowly through a reactor, the microorganism would have a longer residence time and low average UV intensity, which would be found in the upper right quadrant on the contour plot. For each reactor in TABLE 1, fractions of the four quadrants were calculated and compared for the different operating conditions. Additionally, the location of peak fraction points on the contour graph was considered for more detailed analysis when it was difficult to determine which reactor was more efficient.

Experiment

1. UV reactor and pipe fittings

A closed-vessel Schedule 80 PVC reactor was used to validate the data from the CFD model by using a Lagrangian UV sensor developed in our research group which travels through the reactor (Figure 3). The dimension of the reactor was 1ft in diameter, 3ft long and included one LPHO UV germicidal lamp located axially inside the reactor center line.

The lamp power was 87 Watts with 28 Watts UV output at 254nm (catalog number 05-0264 GHO36T5/L/4PSE, Atlantic Ultraviolet Corp.). The water flows through a 6-inch PVC pipe from the inlet side of the reactor to the outlet side. The inlet side 6-inch PVC pipe is connected by a 4-inch pipe, which is 40 inches in length (i.e. 10 pipe diameters) to achieve the straight pipe hydraulic condition. The Lagrangian UV sensor insertion point was composed of a 2-inch pipe, a valve, and a cap. A round rod with a small plate on its end was used to insert the Lagrangian UV sensor into the y-elbow, which was connected to the 4-inch main pipe toward the reactor (Figure 4). The outlet part was composed of 3-inch Tee, 3-inch pipe, a valve, and 90 degree elbow. A net installed inside of the Tee prevented the Lagrangian UV sensor from following water flow toward the recirculation portion of the UV system and forced the Lagrangian UV sensor to the outlet collection point. When the valve of the outlet part was opened, the Lagrangian UV sensor was discharged into a liquid-filled basket (Figure 5).

2. Lagrangian UV sensor (circuit and body)

The body of the Lagrangian UV sensor was made of a quartz shaped tube that was 28mm in diameter and 60mm in length with a cap. The cap was removed in order to place the circuit board into the quartz tube (Figure 6). A bumper was attached on the end of the quartz part to protect both the UV lamp in the reactor and the sensor from breaking when the detector bumped against the lamp or reactor wall. Several weights were added inside of the quartz tube to make the Lagrangian UV sensor neutrally buoyant.

The circuit board was 37mm long and 21mm wide with several mounted components, including a signal microcontroller (MSP430, Texas instruments), two UV sensors (PDU-G106B-SM, Advance Photonix Inc.), silicon phototransistors (OP805SL, Optek Technology, Inc.), amplifiers (TLV2475, Texas instruments) and a battery. Two surface-mounted UV sensors were placed on both sides of the circuit board. A frequency of 60Hz was used to allow for as many readings as possible over a maximum reading time period of 34s. This maximum reading time period was long enough to accommodate the hydraulic residence time of 21s.

3. Collimated Beam Settings

Recordings from the Lagrangian UV sensor provided a digital output between zero and 1024, depending on various voltages received from the UV lamp by the phototransistors. Accordingly, conversion of these digital outputs into UV intensity with units of mW/cm^2 was required. Bench-scale experiments were performed with the collimated beam apparatus (Figure 7) to develop a calibration curve. A UV radiometer was used to measure the output for the lamp in the collimated beam apparatus (UVX Digital radiometer E 27987/ UVP, Inc.). The collimated beam contains four low pressure (LP) UV mercury lamps (catalog number G15T8, Atlantic Ultraviolet Corp.). Both detectors (Lagrangian UV sensor and radiometer) were exposed to the four UV lamps at various distances between 8.5 inches and 16.5 inches at intervals of 0.5 inches. Two calibration curves were developed from two chip-mounted sensors.

4. Pilot Test

The pilot UV system consisted of several components including an 11,000 gallon storage tank filled with tap water, a submersible pump (Model 292 ½ H.P., Zoeller Pump Co., Inc.), a turbine flow meter with flow range capacity of 15-225gpm (±0.50%) (HO2X2-15-225-B-1MX-F1SS, Hoffer Flow Controls), an inlet /outlet for injecting and extracting the Lagrangian UV sensor, several 3-inch PVC ball valves to control the flow, and several ½-inch PVC ball valves to extract air out of the system and LPHO UV reactor. The pilot was operated at 50 (±1) gpm, resulting in hydraulic residence times of 21s in the reactor. Before injecting the Lagrangian UV sensor into the UV system, the UV lamp was warmed up for thirty minutes and the pilot was checked to ensure water filled the entire system. Next the Lagrangian UV sensor was inserted into the inlet by pushing it with a rod. When the Lagrangian UV sensor finished traveling through the UV reactor and reached the outlet, it was extracted from the system by opening the outlet ball valve. The readings of the Lagrangian UV sensor obtained from the UV reactor were transported into the computer by using a receiver apparatus (QSK26A, RENESAS technology)(Figure 8). The same procedures were repeated 100 times to obtain distribution curves for residence time, UV intensity, and UV dose. Finally, three distributions were calculated from modeling data by adjusting the model to the same conditions as the pilot experiments. These were compared to the results from the pilot experiment.

Result and discussion

Modeling data analysis

1. UV dose distribution

According to the UV Disinfection Guidance Manual (2006), one way to qualitatively compare the efficiency between two different UV reactors is to compare the width of the UV dose distribution. In Figure 9, a narrow dose distribution suggests a more efficient reactor, whereas a wider dose distribution indicates a less efficient reactor because it includes lower and higher UV dose regions resulting from short circuiting and recirculation (Cabaj et al., 1996; Sozzi and Taghipour, 2006; USEPA, 2006). The high-dose end of the wider UV dose distribution could suggest an over-dose of treatment, implying a waste of energy. From the standpoint of microorganisms, microbes could retain viability after traversing the irradiated zone in the UV reactor when they take trajectories relatively distant from the lamps (i.e. low-dose end). For example, if 1% of the microorganism receives an insufficient UV dose, then the maximum inactivation of the microorganism would be 99%, irrespective of other aspects of the reactor (Blatchley and Hunt, 1994; Chiu et al., 1999). Thus, it is reasonable to say that broader UV dose indicates a less efficient reactor because of its increased lower UV dose area.

The UV dose distributions were obtained for all four reactor configurations (Figure 10). As expected, a change in the operating conditions caused a corresponding change in the

UV dose distribution. Longer residence times and higher UV intensity made the UV dose distribution wider and shifted the peak location to the right as a result of increased average UV dose. These results are consistent with the calculation of the UV dose, which is the product of the UV intensity and residence time for each microorganism that travels through the reactor. Increasing the residence time or UV intensity, therefore, results in a higher UV dose. For example, in Reactor D, the reactor hydraulics and UV lamp intensity were manipulated at the same time by changing the flow rate and the UV transmittance (UVT). When the flow rate increased from 7.6gpm into 14.4gpm and UVT decreased from 84% to 77% (i.e. condition 2 to condition 1), a narrower UV dose distribution occurred. The peak point in condition 2 was shifted to the left because residence time and UV intensity decreased. Consequently, the average UV dose also decreased because of the decreases in both the residence time and UV intensity (Figure 10-4).

As mentioned earlier, a change in the operating condition for the four different reactors caused a corresponding change of the UV dose distribution curves. However, these different UV dose distributions cannot reveal separately the changed UV intensities and residence times that are directly related to a change in the operating conditions. Therefore, there is a limit to understanding the performance behavior inside the UV reactor by only comparing the width of UV dose distribution curves.

2. Residence time distribution (RTD)

Figure 11 displays the RTD curves for Reactors A-D. In Figure 11, all of the RTD curves for the four reactors had peak points at different times on the x-axis and different widths of RTD curve as flow rate conditions changed. As expected, slower flow rates produced longer residence times, which made RTDs wider and shifted the peak location to the right. For the four Reactors, the RTD curves in conditions with slowest flow rate (i.e. conditions 1, 1, 3, and 1 for Reactor A, B, C, and D, respectively) were located to the right of other conditions with a broader width.

When comparing the residence time coefficient of variation (CV_t), all reactors had different CV_t with a change of flow rate. With the exception of some cases (condition 2 for Reactor A, condition 2 for Reactor B, and both conditions for Reactor D), the CV_t increases with decreasing flow rate, which means Reactor A-C reduces its hydraulic efficiency with decreasing flow (TABLE 2). Reactor A and C can be operated most similarly to ideal PFR at conditions 3, 2 respectively, at the highest flow rate. Reactor D seems to have better hydraulic efficiency with decreasing flow. From the CV_t distribution plots, most of the differences in CV_t occurred below CV_t of 0.3, while fractions for CV_t above 0.5 were almost the same (Figure 12).

When comparing the fractions of lower residence times with average residence times, the fractions were very similar in terms of each reactor as its operating condition was changed. However, different reactors had various fractions that resulted from variations

in reactor configurations. These variations included various lamp arrangements within the reactor and different combinations of pipe and fittings upstream from the UV reactor. Based on the fraction of residence time, Reactor A had the largest fraction with a residence time lower than average and Reactor D had the smallest (TABLE 2). Short residence times could produce low UV doses. However, provided that a combination of residence time and UV intensity forms the required UV dose for disinfection, a reactor with a larger fraction of residence times lower than the average may be more efficient if it comes with a higher fraction of UV intensities above the average UV intensity. Because individual microorganisms with a certain amount of residence time can have various average UV intensities through the reactors, it is insufficient to explain the reactor performance with only the residence time distribution. The analysis considering the relationship between the residence time and the UV intensity was performed and the results were displayed with contour plots showing the fraction of microorganisms at a certain residence time and a certain average UV intensity during travel through the reactor.

3. UV intensity distribution

Figure 13 displays the UV intensity distribution for the four reactors discussed in the previous section. In Figure 13, the curve for Reactor A/condition 4 was shifted significantly to the right in the high UV intensity region compared to the other operating conditions because all eight lamps with 70% power were used. Conversely, the UV intensity curve for condition 2 was located primarily in the low UV intensity regions

because only five lamps operating at 58% power were used. In the case of Reactor B, the UV transmittance was changed to produce different UV intensities in conditions 2, 3, and 4. Among the three conditions, condition 3 had the highest UV transmittance, 95.5%, which explains the high UV in the UV intensity distribution range. The UV intensity curve for condition 1 had the lowest UV intensity range because of the low power supplied to the lamps. For Reactor C, three banks containing lamps were used to set different UV intensity conditions. In condition 1, all lamps in bank 1 were on. In condition 2, all lamps in banks 1 and 2 were operated. Finally, condition 3 represents all lamps on in banks 1 – 3. The results in Figure 13-3 for Reactor C clearly show the expected shift in the UV intensity to higher UV intensity values with the number of banks turned on. In the case of Reactor D (Figure 13-4), a higher UV transmittance (84% UVT) was used for condition 1 compared to condition 2 (77% UVT). Consequently, the UV intensity distribution was located at a higher UV intensity region for condition 1 compared to condition 2.

Comparing the UV intensity coefficients of variation (CV_I) for each condition, Reactor A has the smallest CV_I (0.437) at condition 4 and the largest CV_I (0.784) at condition2 (TABLE 2). Likewise, Reactor B, C and D had small CV_I values at condition 3, 3, and 1 respectively, based on UV intensity field. When comparing different reactors in TABLE 1, Reactor C overall has the smallest average CV_I and Reactor A has the largest average CV_I. Therefore, Reactor C produced the closest UV intensity distribution to an ideal PFR among four reactors based on CV_I. Consequently, microorganisms traveling through Reactor C would likely receive a consistent UV intensity field close to average. In

contrast, microorganisms in Reactor A which had the largest CV_I had a wider range of UV intensities relative to the average UV intensity for the reactor compared to other reactors in this study. Therefore, microbes in Reactor A would receive a wide range of UV intensities and an inefficient level of UV dose depending on the path taken through the reactor. Like the CV_t distribution analysis, most of differences of the CV_I between the different reactors resulted from the different fraction in small CV_I (Figure 14). The CV_I plot for Reactor A showed different fractions in broad CV_I region between 0 and 1 unlike other CV_I plots for Reactor B, C and D, which had different fractions in CV_I below 0.5.

When comparing the fraction of higher UV intensity than average for the different reactors, the values did not change significantly for Reactor B and Reactor D under different conditions reported in this study. With respect to Reactor A, however, the difference between the fractions at condition 3 and 4 was not negligible. In the case of Reactor C, the fraction kept increasing as the conditions were changed. These results are likely from different arrangements of the UV lamp. Reactor B and Reactor D had similar lamp arrangements parallel to flow direction. In Reactor A, the UV lamps were arranged vertical to flow direction and Reactor C had three banks of UV lamps connected axially and arranged parallel to flow so that each bank's UV lamps were on or off as the conditions were changed. Based on the fraction of UV intensity, Reactor C at condition 3 had the largest fraction, 0.46. The results indicate that most microbes in Reactor C under condition 3 took more desirable paths for disinfection because they traveled through the reactor close to the UV lamp. So, Reactor C was the most effective among the 4 reactors in terms of the fraction of UV intensity when all banks were operated. However, similar

to the previous RTD analysis, the analysis of the UV intensity field alone is insufficient to explain the reactor performance. Additional analysis considering the relationship between RTD and UV intensity distribution may explain the reactor performance more accurately.

4. Relationship between residence time and UV intensity

In Figure 2, quadrant 2 could be regarded as an undesirable condition for microbes since these organisms take trajectories with longer residence times and low UV intensities. Quadrant 2 indicates that they take an undesirable path close to the wall. In contrast, quadrant 3 could be a preferred condition for microorganisms because it represents paths through the reactor with shorter residence times and high UV intensities. In other words, microbes in this quadrant could take more desirable paths by staying in the reactor for as little time as possible and traveling close to the lamp. Therefore, UV reactor efficiency would increase by having a higher fraction of paths with lower residence time and high average UV intensity, and a lower fraction of paths with longer residence time and low average UV intensity. Designers that analyze the reactor performance and make design modifications that lead to the increase of microbes in quadrant 3 while decreasing the number of microbes in quadrant 2 could develop reactors with lower operating cost (i.e., lower lamp power) and a smaller footprint (i.e., lower HRTs) to achieve the same required dose.

For all reactors, a large fraction of microbes were located in quadrant 1 with the exception of Reactor D (TABLE 3). The result in TABLE 3 indicates that many microbes took paths close to the wall in the reactor and passed through the reactor very quickly. Reactor A had very similar fractions in four quadrants under several operating conditions. Under condition 2, Reactor A had the smallest fraction in quadrant 2 (an undesirable condition) and had the largest fraction in quadrant 3 (a preferred condition) under condition 4.

The location of the peak point in Figure 15 was used as an assessment point when it was difficult to assess which condition was more efficient for the reactor. The peak point was shown as a coordinate with a normalized residence time on the x-axis and a normalized UV intensity on the y-axis. Therefore, when the coordinate is (1, 1), microorganisms at this point traveled into the reactor with average residence time and UV intensity. The distance from this (1, 1) position to the peak location was computed for each condition since this could serve as an estimate of the effort required to achieve a UV reactor design with plug flow characteristics. Under condition 2, the peak point was located at the coordinate (0.8, 0.2) (distance = 0.825) while other conditions had peak points at the coordinate of (0.8, 0.6)(distance = 0.447). These results indicated more microorganisms under condition 2 took paths with lower UV intensities than under other test conditions. In the case of Reactor A (Table 3), condition 4 was the best for the reactor's operation because it had the largest fraction in quadrant 3 (a preferred condition) and a relatively small fraction in quadrant 2 (an undesirable condition). Reactor A results agreed to CV_I analysis in TABLE 2 since Reactor A had the smallest CV_I of 0.437 under condition 4.

The combined contour plot and CV_I results imply that Reactor A operated at the highest UV intensity efficiency under condition 4.

Reactor B had also very similar fractions in the 4 quadrants under the 4 different test conditions (Table 3). Compared with Reactor B (condition 2), condition 4 had a lower fraction in quadrant 2 (an undesirable condition) as well as a lower fraction in quadrant 3 (a preferred condition). It was difficult to evaluate which condition was more efficient for this reactor operation based solely on the contour plot analysis, since the peak points for all conditions were also the same at the coordinate of (0.8, 0.8). No significant data was provided by the CV_I analysis in Table 2 to help determine the better operating condition for Reactor B. Reactor C had the largest fraction in quadrant 3 and the smallest fraction in quadrant 2 under condition 3. Reactor D had very similar fractions in the four quadrants under both test conditions. But based on the peak point location, Reactor (condition 1) was better than condition 2 because the peak point (coordinate of (1, 0.6))(distance = 0.4) for condition 1 indicated higher normalized UV intensity than condition 2, which had the peak point at coordinate (1.1, 0.4)(distance = 0.608).

5. Comparison between two reactors with similar UV dose distribution

An additional analysis of Reactor B (condition 4) and Reactor D (condition 1) was performed since they each had an operating condition that resulted in similar UV dose distributions (Figure 16). Based on the UV dose distribution, both reactors should have relatively similar performance efficiency. However, analysis of the residence time and

UV intensity contour plots displayed significant differences between these two reactors (Figure 16 b) and c)). In the contour plot for Reactor B, the peak point was located at the coordinate of (0.8, 0.8)(distance = 0.283) with a majority of the data in quadrant 1. In the contour plot for Reactor D, most of the data was located in quadrant 2 and the peak point was located at the coordinate of (1.1, 0.6)(distance = 0.412). From the disinfection point of view, quadrant 1 (short residence time and low UV intensity) also needs to be considered carefully since the trajectories in quadrant 1 would result in a low UV dose region within the UV dose distribution. However, both reactors had similar low UV dose region in the UV dose distribution so that the fraction in quadrant 1 had little influence on deciding which reactor had an overall more efficient performance.

Compared to Reactor D, Reactor B had both strengths and weaknesses based on analyzing the results in quadrants 2 and 3 (undesirable condition and preferred condition, respectively) on the contour plot. In TABLE 3, for Reactor D, a higher fraction of microbes was found in quadrant 3 (preferred condition) while Reactor B displayed a lower fraction of microorganisms in quadrant 2 (undesirable condition). Clearly, contour plots can help describe the specific hydrodynamics and UV intensity distributions for each reactor and have the potential for improving the reactor design by changing desired conditions (e.g. arrangement of UV lamps, reactor design shape) to reduce and increase fractions in quadrant 2 and 3, respectively.

Analysis of Lagrangian UV sensor

1. Collimated beam test

As mentioned earlier, the two individual sensors, which make up the Lagrangian UV sensor device, were analyzed with the collimated beam apparatus. Although both sensors were made by the same manufacturer, individual sensors responded differently in the presence and absence of UV light. From both sensor readings and radiometer readings, two calibration curves were produced (Figure 17). Using these equations, reading values from the Lagrangian UV sensor were converted to UV intensity with unit of mW/cm^2.

$$y_1 = 0.0016x_1 - 0.038 \text{ (for sensor1)}, \quad (5)$$

$$y_2 = 0.0017x_2 - 0.037 \text{ (for sensor2)} \quad (6)$$

(y = UV intensity (mW/cm2), x = readings from Lagrangian UV sensor)

Sensor readings below 23.054 for sensor 1 and 21.59 for sensor 2 were considered zero for purposes of calculating average UV intensity in the pilot test.

2. Pilot test

From one run of the Lagrangian UV sensor through the pilot UV system, 2046 readings were obtained with 1/60s recording time for each reading. The average UV intensities were calculated by averaging the calibrated UV intensities from both sensors. 100 injections of the Lagrangian UV sensor were used to produce residence times and

average UV intensities. This total number of the injections was chosen because the results showed little difference when 70 injections were used compared to 100 injections (Figure 18). The product of the individual residence times and average UV intensities were used to compute the individual UV doses. Three distribution plots (residence time, UV intensity and UV dose) were developed from the 100 injections of the Lagrangian UV sensor (Figure 18). Table 4 displays the average residence times, average UV intensities, and average UV doses for a reactor.

These distributions and average values from the pilot test were compared with the results from the modeling data under the same operating conditions. In TABLE 4, the average residence time in the pilot test was 34% higher and the residence time distribution curve was much broader than the model predictions (Figure 18 and 19). The difference between the Lagrangian UV sensor results and the modeling results is likely due to the larger size of the Lagrangian UV sensor, which might produce a more irregular path during its travel through the reactor compared to significantly smaller microorganisms. This differing path dynamics taken by the Lagrangian UV sensor may lead to a broader residence time distribution curve (the range between 1.7s and 34.1s) compared to the distribution curve (the range between 9.58 and 15s) obtained from modeling data. The model predicted similar results to experimental microspheres work performed in Zhao (2007) with the same UV reactor configuration and operating conditions.

The average UV intensity obtained with the Lagrangian sensor was about 9% lower than average UV intensity predicted from the model. This lower average UV intensity might be due to several limitations:

1) two sensors placed 180˚ apart with a limited view angle which do not simulate the 360˚ reception achieved by microorganisms;

2) the irregular path taken by the sensor described previously as well as the sensor moving in an upward stance configuration (Figure 20). This upward stance may still limit the true UV intensity received by the microorganism as it moves through the UV reactor;

3) when the UV light was irradiated to the edges of the circuit board, the UV light was outside the range of the sensor view window and resulted in a blind spot where nothing was recorded;

4) the UV sensor could not measure higher UV intensities than about 1.95mW/cm^2. All UV intensities higher than 1.95mW/cm^2 were recorded as an identical intensity of 1.95mW/cm^2.

Despite these limitations, this experimental method using the Lagrangian UV sensor showed that it was possible to measure UV intensity and residence time. If these limitations are fixed by making a smaller Lagrangian UV sensor with more UV sensors that can cover the entire sensor chamber surface area irradiated by the UV lamp and by changing settings on the circuit board to measure maximum UV intensity from the UV lamp in the pilot test, modeling data can be better verified in terms of UV intensity and residence time.

Conclusion

A study has been performed to evaluate performance of the UV reactor by analyzing the residence times and UV intensities modeling data and by developing an experimental method to measure them. Fractions of normalized residence time and UV intensity from different UV reactors were calculated and displayed by contour graphs. Coefficients of variation (CV) for residence time and UV intensity were also calculated using the modeling data. The results showed that reactors with smaller UV intensity CVs displayed higher UV reactor performance efficiencies. For most cases, these results agreed with the results from comparing fractions in the contour plots. Two reactors with very similar UV dose distribution curves produced significantly different contour plots displaying the fractions of the microorganisms with a certain residence time and a certain average UV intensity through the reactor. The Lagrangian UV sensor was used in the pilot test to measure the residence time and UV intensity of microorganisms moving though a UV reactor. Because the Lagrangian UV sensor used in the pilot test had several limitations for measuring UV intensity and residence time correctly, there were some discrepancies between the pilot test results and the modeling data. However, this method has the potential to experimentally measure residence time and UV intensity at the same time. Overall, the analysis with RTD and UV intensity distribution produced a more detailed explanation of the UV reactor performance compared to analysis of UV dose distribution alone.

References

Anderson, W.A., Zhang, L., Andrews, S.A., Bolton, J.R. (2003) “A technique for direct measurement of UV fluence distribution.” *In Proceedings of the Water Quality Technology Conference*; American Water Works Association: Philadelphia, PA, 2003.

Batchley, E.R. III.,Wood. W.L., Schuerch, P. (1995) “UV Pilot Testing: Intensity Distributions and Hydrodynamics” J. Environ. Eng., 121(3), 258-262.

Blatchley, E.R. III., Hunt, B.A. (1994) “Bioassay for Full-scale UV Disinfection systems” *Wat. Sci. Tech*., 30, 115-123.

Blatchley, E., Shen, C., Naunovic, Z., Lin, L., et al. (2006) “Dyed Microspheres for Quantification of UV Dose Distributions: Photochemical Reactor Characterization by Lagrangian Actinometry.” *J. Environ. Eng*., 132(11), 1390-1403.

Blatchley, E.R. III., Shen, C., Scheible, O.K, Robinson, J.P., Ragheb, K., Bergstrom, D.E., Rokjer, D. (2008) ”Validation of Large-scale, monochromatic UV disinfection systems for drinking water using dyed microspheres” *Wat. Res*., 42, 677-688.

Bohrerova, Z., Bohrer, G., Mohanraj. S.M., Ducoste, J.J., Linden. K.G. (2005) “Experimental Measurements of Fluence Distribution in a UV Reactor Using Fluorescent Microspheres” *Environ. Sci. Technol*., 39, 8925-8930.

Cabaj, A., Sommer, R., Schoenen, D. (1996) “Biodosimetry: Model Calculations for UV water disinfection Devices with regard to Dose Distributions” *Elsevier Sci*., 30, 1003-1009.

Chiu, K, Lyn, D.A., Savoye, P., Blatchley, E.R. III. (1999) “Integrated UV disinfection model based on microorganism tracking” *J. Environ. Eng*, 125(1), 7-16.

Clark, M.C. (1996) “Transport Modeling For Environmental Engineers and Scientists” *Environmental science and technology.*

Ducoste, J.J. and Linden, K.G., (2006) “Hydrodynamic Characterization of UV Reactor.” *American Water Works Association Research Foundation*, Denver, Co.

Ducoste, J.J., Liu, D., Linden, K. (2005) “Alternative Approaches to Modeling Fluence Distribution and Microbial Inactivation in Ultraviolet Reactors: Lagrangian versus Eulerian” *J. Envron. Eng*., ASCE, 1393-1403.

Janex, M.L., Sayoye, P., Do-Quang, Z., Blatchley, E., Laine, J.M. (1998) “Impact of water quality and reactor hydrodynamics on wastewater disinfection by UV, use of CFD modeling for performance optimization.” *Water Sci. Technol*. 38 (6), 71-78

Lin, L-S and Blatchley, E.R III. (2001) “UV dose distribution characterization using fractal concepts for system performance evaluation” *Water Sci. Technol*., 43, 181-188.

Lyn, D.A., Blatchley III, E.R. (2005) “Numerical computational fluid dynamics-based models of ultraviolet disinfection channels.” *J. Environ. Eng*., ASCE 125 (1), 17-26.

Sozzi, D.A and Fariborz Taghipour. (2006) “UV Reactor Performance Modeling by Eulerian and Lagrangian Methods.” *Environ. Sci. Technol.*, 40, 1609-1615.

Qualls, R.G., and Johnson, J.D. (1983) “Bioassay and dose measurement in UV disinfection.” *Appl. Environ. Microbiol.*, 45(3), 872–877.

Unluturk. S.K., Arastoopour, H., Koutchma, T. (2004) “Modeling of UV dose distribution in a thin-film UV reactor for processing of apple cider” *J. food eng.* 65. 125-136

USEPA (2006) EPA 815-R-06-007 “Ultraviolet Disinfection Guidance Manual for the Final Long Term 2 Enhanced Surface Water Treatment Rule.” November 2006, *USEPA, Office of Water(460).*

Zhao Xi (2007) “Analysis of a Low Pressure UV reactor under Multiple pstream Elbow Configurations using UV Sensitive Fluorescent Microspheres” thesis in Department of Civil, Construction, and Environmental Engineering in NCSU

TABLE 1: Operating conditions for four different reactors

		Flow rate	UVT (%)	Lamp power		etc
Reactor A	Condition 1	8.6mgd	90.3	2.8KW	70%	6 lamps on
	Condition 2	8.7mgd	89.6	2.8KW	58%	5 lamps on
	Condition 3	9.9mgd	89.1	2.8KW	61%	7 lamps on
	Condition 4	10mgd	90.9	2.8KW	70%	8 lamps on
Reactor B	Condition 1	1.0mgd	97.9	230W	34%	
	Condition 2	6.34mgd	89.3	230W	100%	
	Condition 3	8.87mgd	95.5	230W	100%	
	Condition 4	8.87mgd	94	230W	100%	
Reactor C	Condition 1	3.3(mgd)	74	230W	100%	1 bank on
	Condition 2	3.3(mgd)	74	230W	100%	2 banks on
	Condition 3	1.9(mgd)	74	230W	100%	3 banks on
Reactor D	Condition 1	7.6 gpm	84	9.5W	100%	
	Condition 2	14.4 gpm	77	9.5W	100%	

TABLE 2: Coefficients of Variation (for time and UV intensity) and fraction of less residence time and higher UV intensity than average for four different reactors with several operating conditions

		Average residence time (sec)	Average UV intensity (mW/cm^2)	CV of Time (CV_t)	The fraction of Less residence time than average	CV of intensity (CV_I)	The fraction of higher UV intensity than average
Reactor A	Condition 1	4.57	25.40	0.181	0.72	0.544	0.35
	Condition 2	4.29	18.00	0.202	0.74	0.784	0.34
	Condition 3	3.65	25.51	0.162	0.69	0.519	0.32
	Condition 4	4.17	33.57	0.175	0.73	0.437	0.38
Reactor B	Condition 1	17.09	6.80	0.213	0.68	0.363	0.34
	Condition 2	6.15	8.62	0.171	0.68	0.379	0.35
	Condition 3	4.33	14.82	0.196	0.68	0.361	0.34
	Condition 4	4.33	11.95	0.196	0.68	0.366	0.34
Reactor C	Condition 1	6.45	1.95	0.076	0.61	0.388	0.35
	Condition 2	6.43	4.88	0.048	0.59	0.344	0.42
	Condition 3	11.48	6.10	0.085	0.61	0.280	0.46
Reactor D	Condition 1	4.42	11.46	0.232	0.52	0.414	0.37
	Condition 2	2.33	9.46	0.297	0.52	0.487	0.37

TABLE 3: Fractions in four quadrants on the contour plot for four different reactors with several operating conditions

		quadrant 1	quadrant 2	quadrant 3	quadrant 4
Reactor A	Condition 1	0.49	0.16	0.23	0.12
	Condition 2	0.53	0.13	0.21	0.13
	Condition 3	0.50	0.18	0.19	0.13
	Condition 4	0.48	0.14	0.25	0.13
Reactor B	Condition 1	0.51	0.15	0.17	0.17
	Condition 2	0.50	0.15	0.18	0.17
	Condition 3	0.51	0.15	0.16	0.18
	Condition 4	0.51	0.14	0.17	0.18
Reactor C	Condition 1	0.38	0.27	0.23	0.12
	Condition 2	0.31	0.27	0.28	0.14
	Condition 3	0.31	0.24	0.30	0.16
Reactor D	Condition 1	0.27	0.35	0.25	0.12
	Condition 2	0.27	0.36	0.25	0.12

TABLE 4: Results (Average residence time, Average UV intensity and Average UV dose) from pilot test and modeling data

	Average residence time(sec)	Average UV Intensity (mW/cm2)	Average UV dose (mJ/cm2)
Pilot test (70 injections)	17.74	0.43	7.66
Pilot test (100 injections)	16.61	0.41	6.86
Modeling result	12.2	4.59	56.24

Reactor A

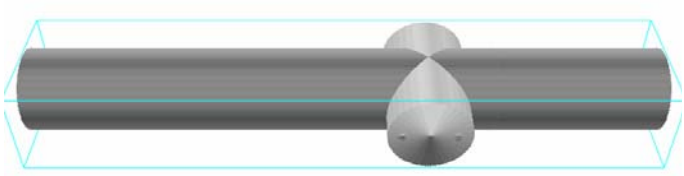

Reactor B

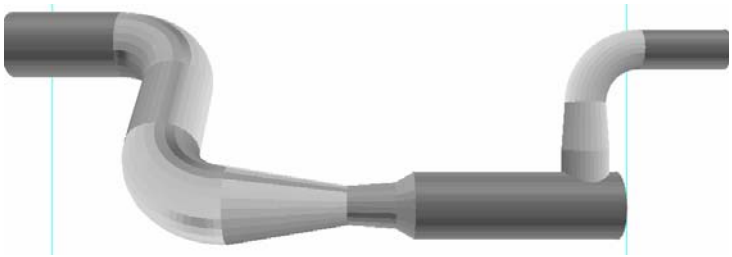

Reactor C

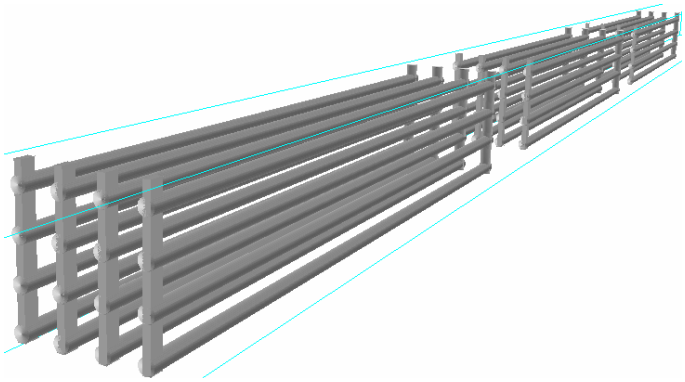

Reactor D

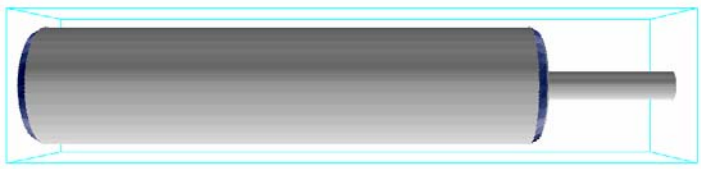

Figure 1: Schematics of four reactors

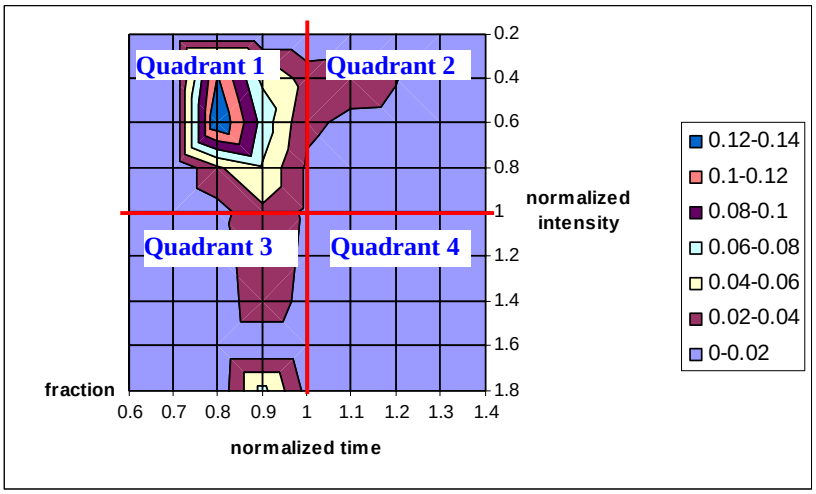

Figure 2: Contour plot as a new method for analyzing data about 1,500 microorganisms with certain combinations between residence time and UV intensity

Figure 3: Photograph of pilot test that displaying injecting and excluding Lagrangian UV sensor

Figure 4: Inlet part that Lagrangian UV sensor enter into the UV system

Figure 5: Outlet part that Lagrangian UV sensor get out of the UV system

Figure 6: Quartz tube as a Body of Lagrangian UV sensor

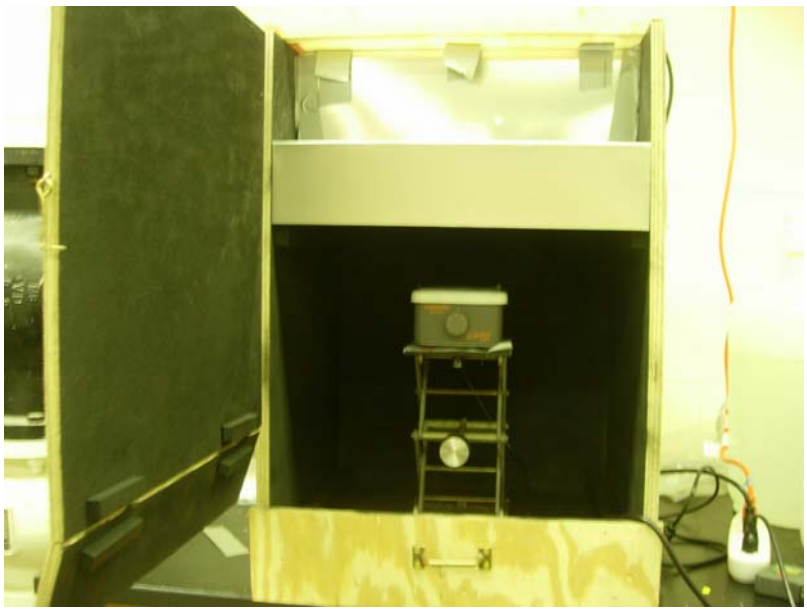

Figure 7: Collimated beam apparatus

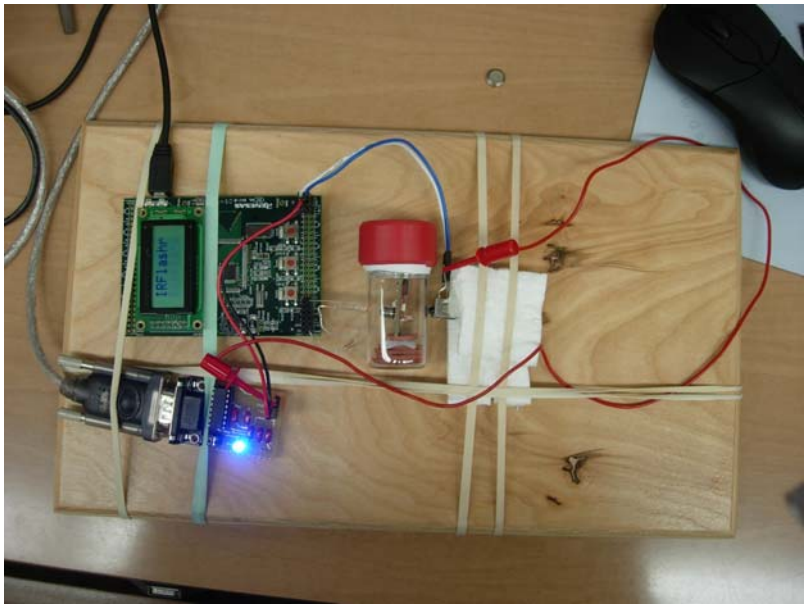

Figure 8: data receiver apparatus

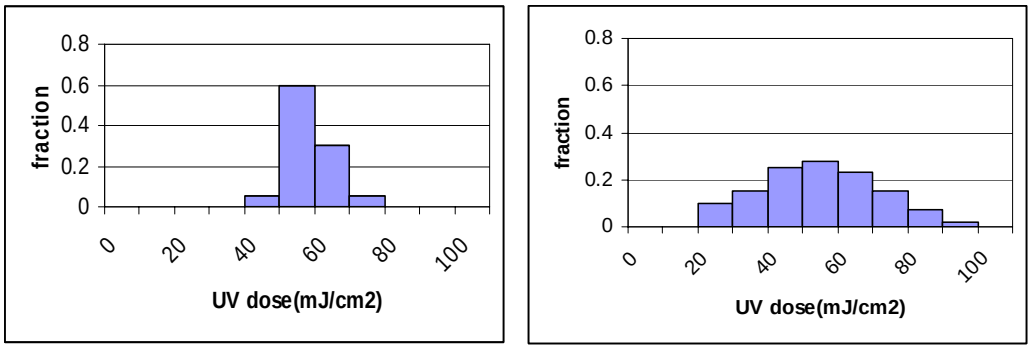

Figure 9**:** Hypothetical UV dose distribution for two reactors with different hydraulics (left : narrow dose distribution, near Plug-flow condition, right : wide dose distribution, poorer hydraulic condition)

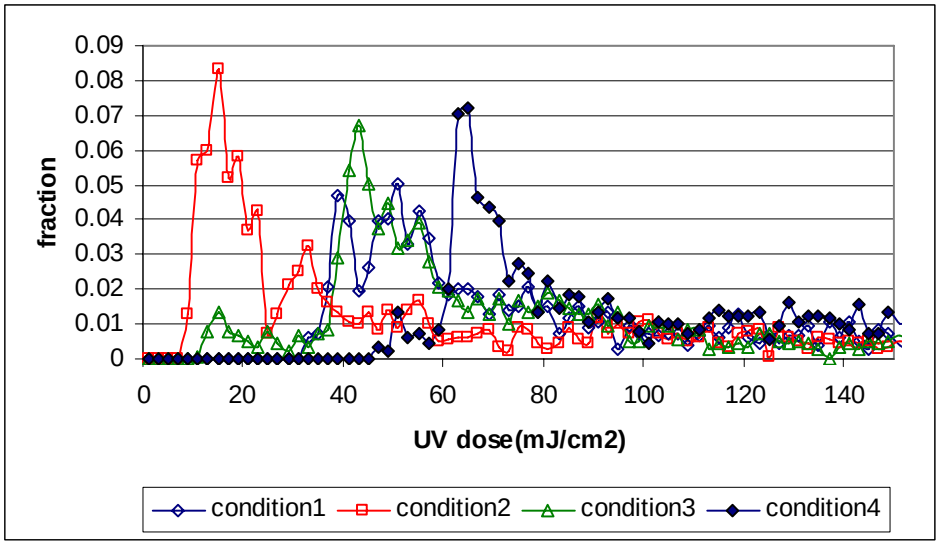

Figure 10-1: UV dose distributions for Reactor A

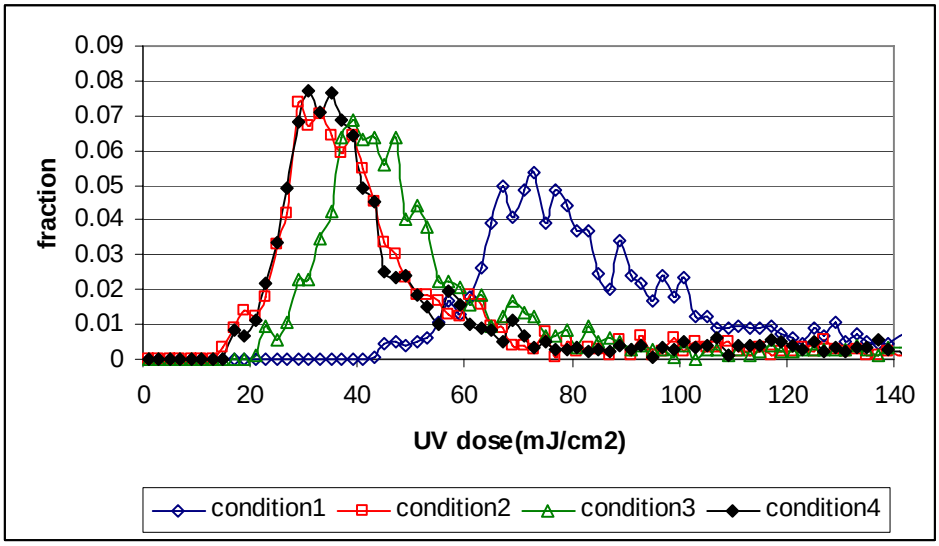

Figure 10-2: UV dose distributions for Reactor B

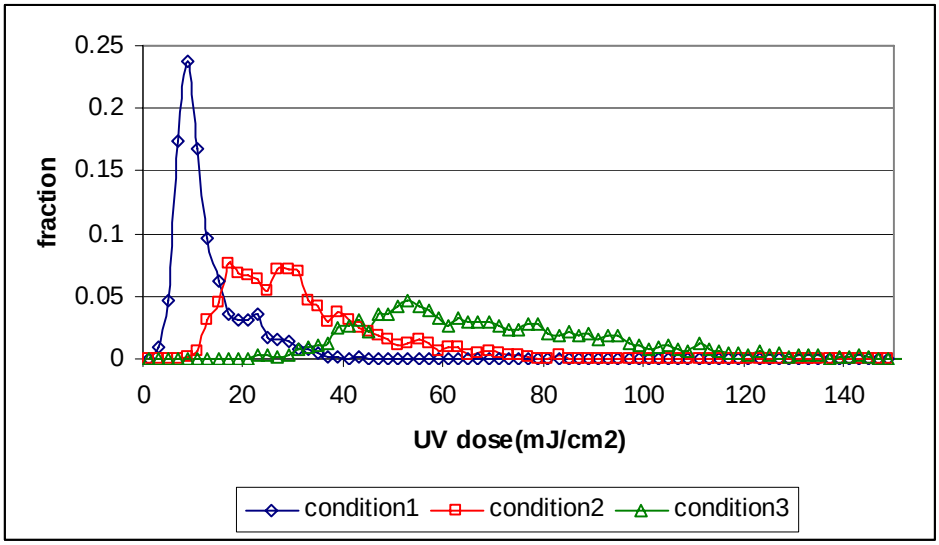

Figure 10-3: UV dose distributions for Reactor C

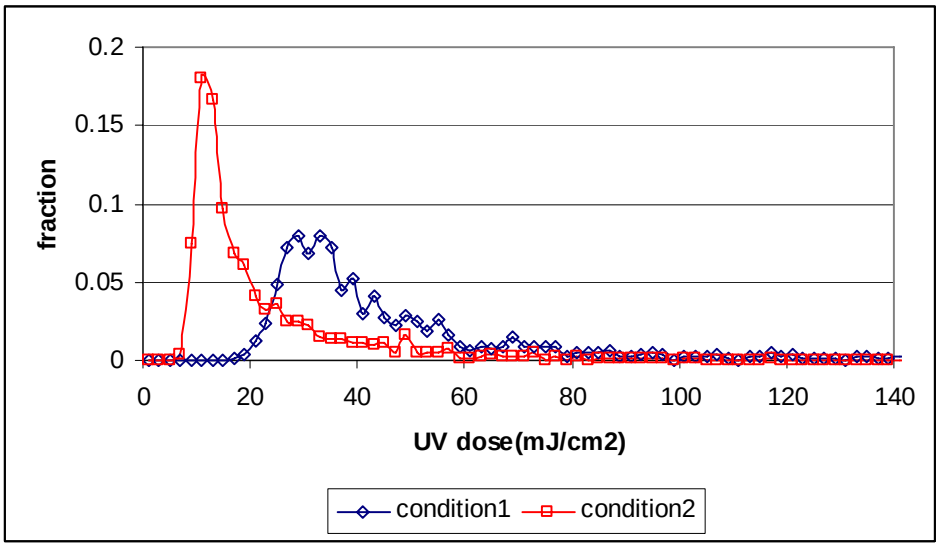

Figure 10-4: UV dose distribution for reactor D, Condition 1) flow = 7.6gpm, UVT = 84% Condition 2) flow =14.4gpm, UVT = 77%

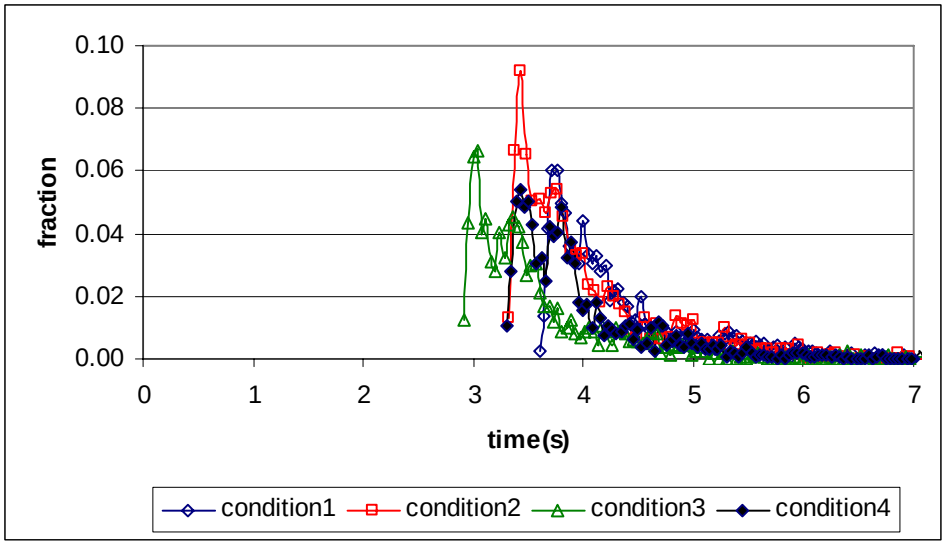

Figure 11-1**:** Residence time distribution for Reactor A under 4 different conditions, condition 1) flow = 8.6MGD, condition 2) flow = 8.7MGD, condition 3) flow = 9.9MGD, condition 4) flow = 10 MGD

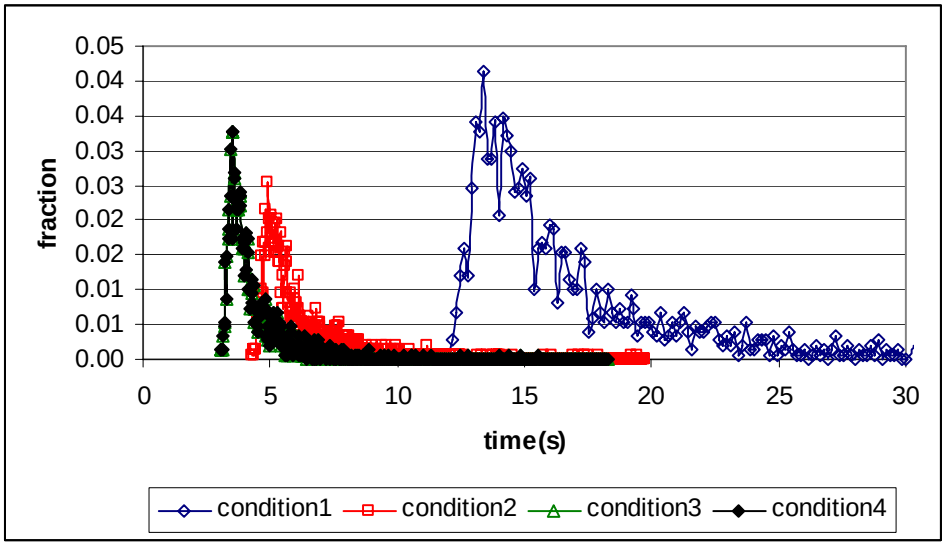

Figure 11-2: Residence time distribution for Reactor B under 4 different conditions, condition 1) flow = 1.0MGD, condition 2) flow = 6.34MGD, condition 3) flow = 8.87MGD, condition 4) flow = 8.87MGD

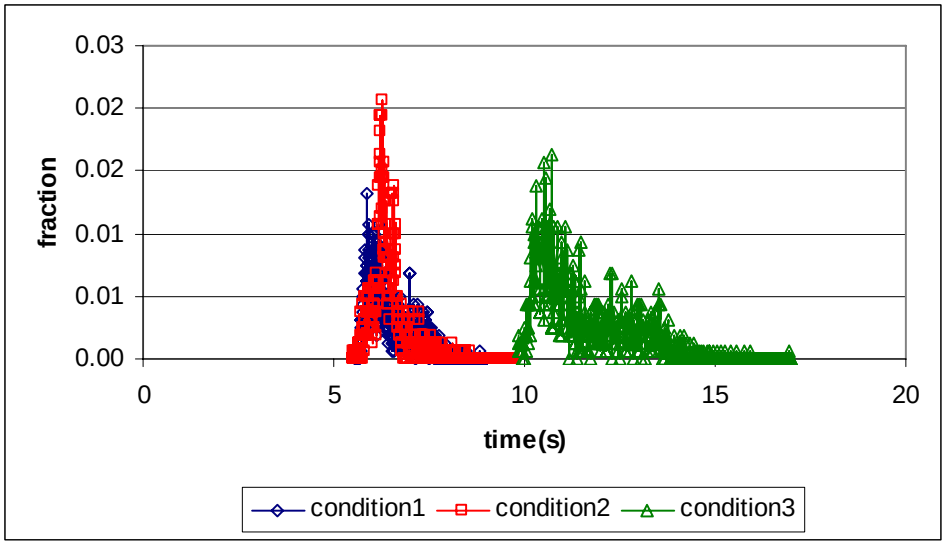

Figure 11-3: Residence time distribution for Reactor C under 3 different conditions, condition 1) flow = 3.3MGD, condition 2) flow = 3.3MGD, condition 3) flow = 1.9MGD

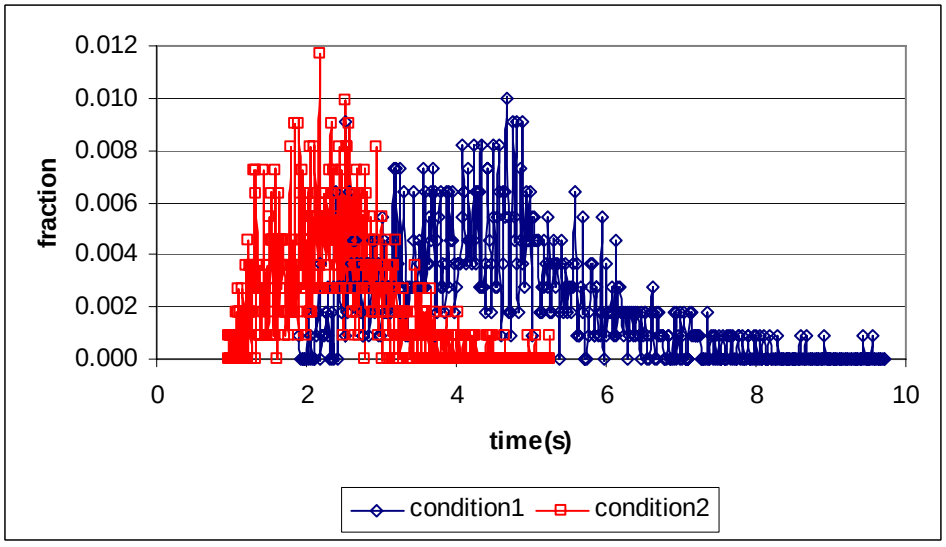

Figure 11-4: Residence time distribution for Reactor D under 2 different conditions, condition 1) flow = 7.6GPM, condition 2) flow = 14.4GPM

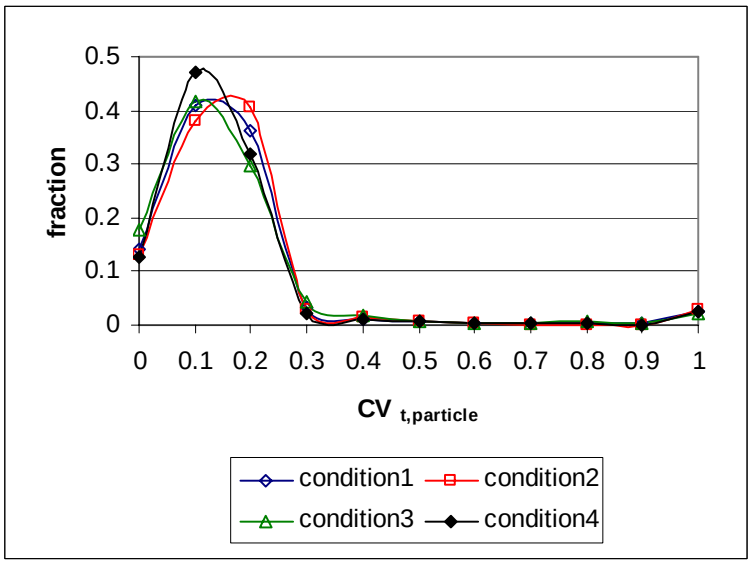

Figure 12-1: Coefficient of Variation plots about residence time for Reactor A

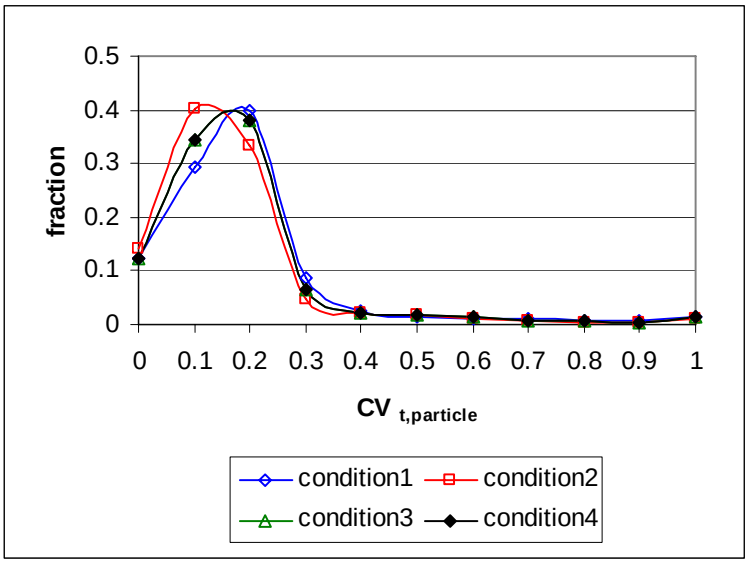

Figure 12-2: Coefficient of Variation plots about residence time for Reactor B

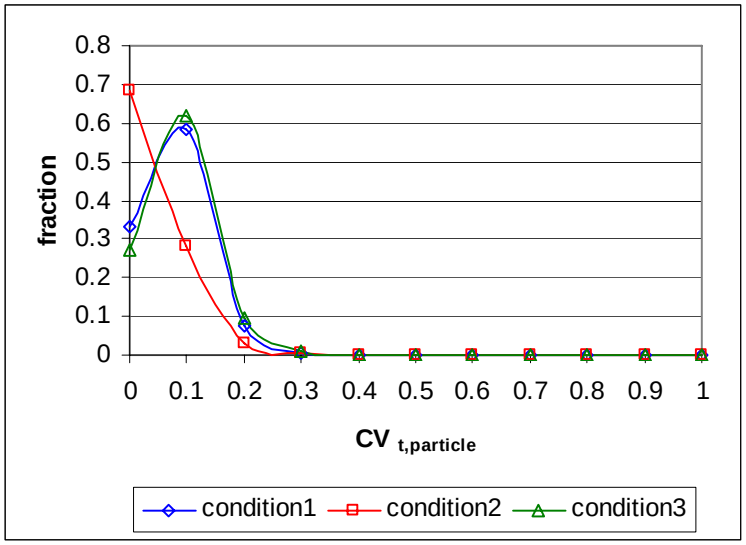

Figure 12-3: Coefficient of Variation plots about residence time for Reactor C

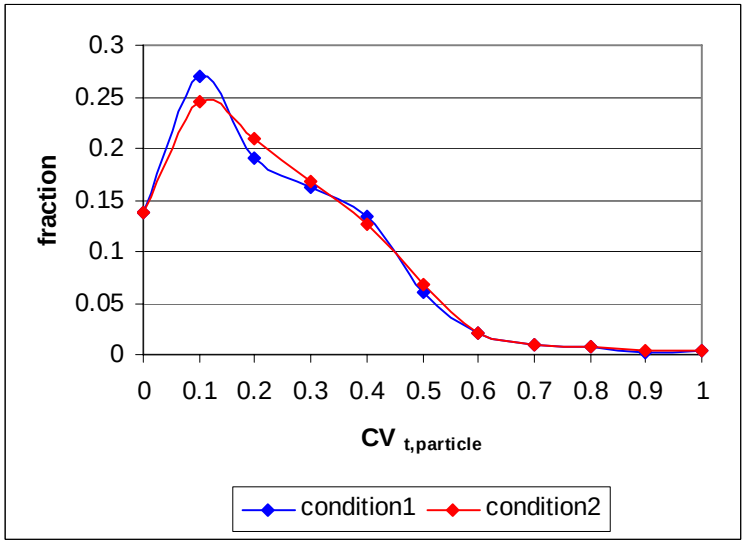

Figure 12-4: Coefficient of Variation plots about residence time for Reactor D

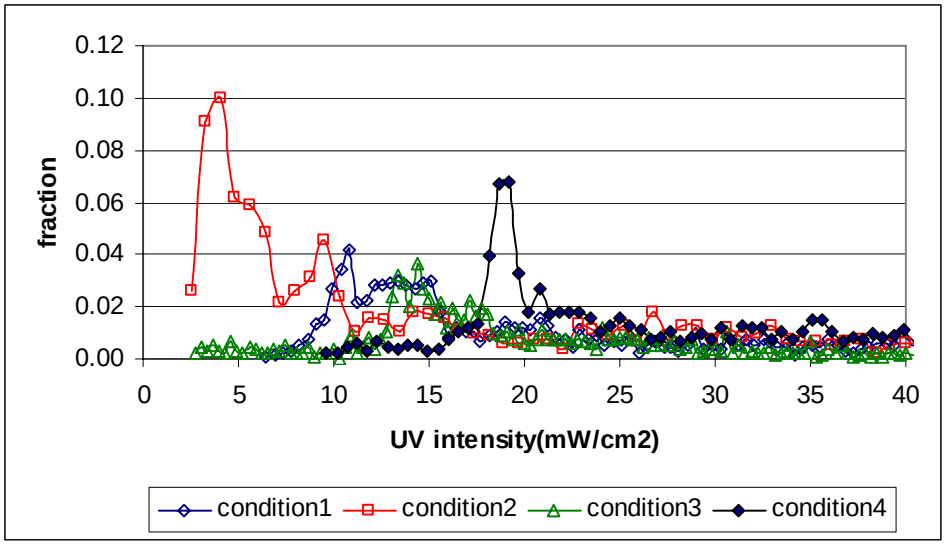

Figure 13-1: UV intensity distribution for Reactor A under 4 different conditions, condition 1) UVT = 90.3%, lamp power = 70%, condition 2) UVT = 89.6%, lamp power = 58%, condition 3) UVT = 89.1%, lamp power = 61%, condition 4) UVT = 90.9, lamp power = 70%

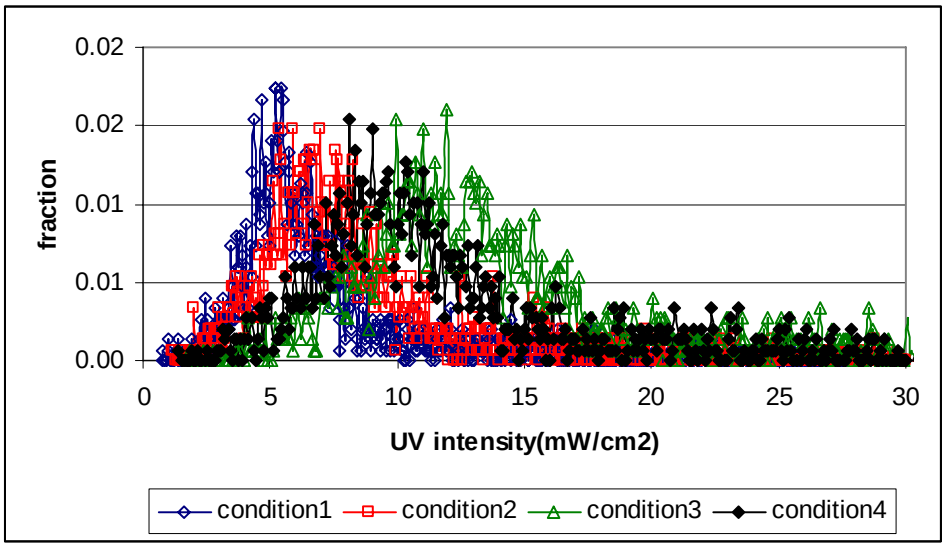

Figure 13-2**:** UV intensity distribution for Reactor B under 4 different conditions, condition 1) UVT = 97.9%, lamp power = 34%, condition 2) UVT = 89.3%, lamp power = 100%, condition 3) UVT = 95.9%, lamp power = 100%, condition 4) UVT = 94, lamp power = 100%

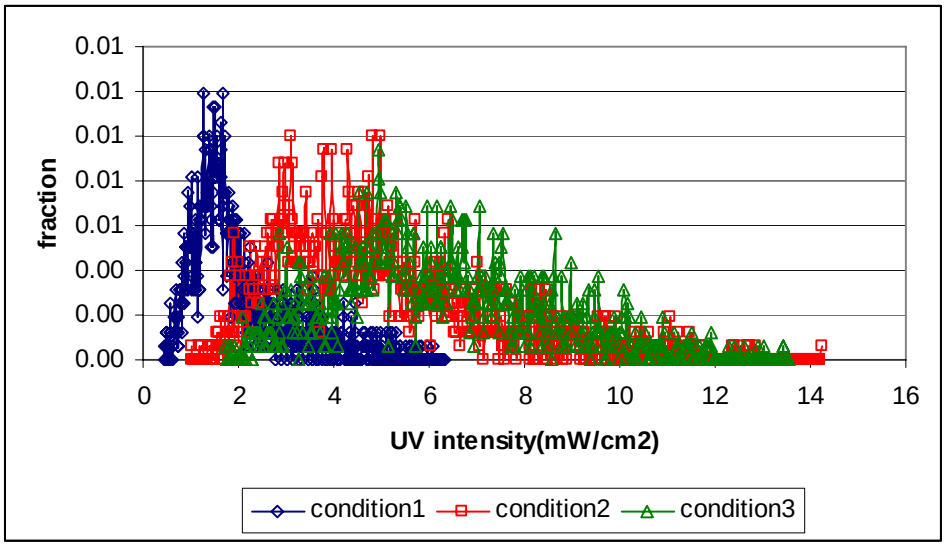

Figure 13-3: UV intensity distribution for Reactor C under 3 different conditions, condition 1) UVT = 74%, 1 bank on, condition 2) UVT = 74%, 2 banks on, condition 3) UVT = 74%, 3 banks on

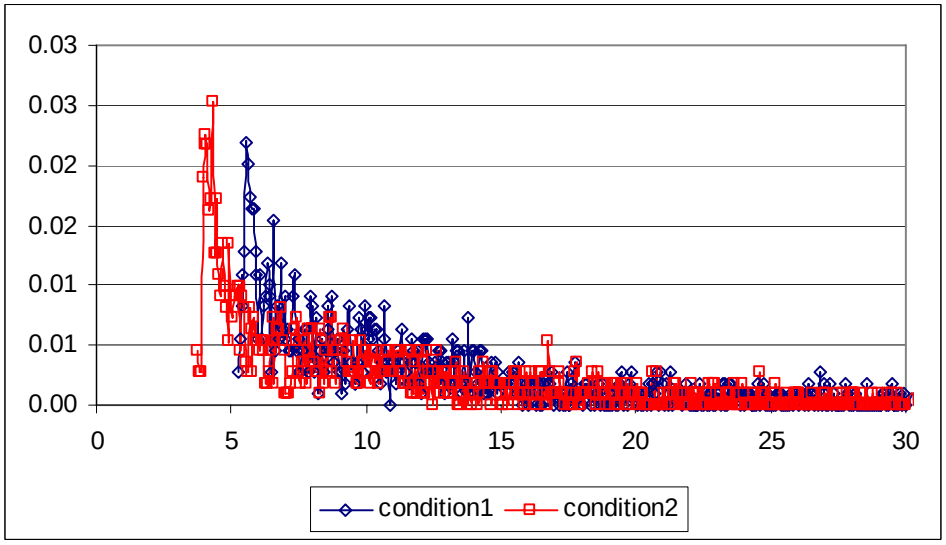

Figure 13-4: UV intensity distribution for Reactor D under 2 different conditions, condition 1) UVT = 84%, lamp power = 100%, condition 2) UVT = 77%, lamp power = 100%

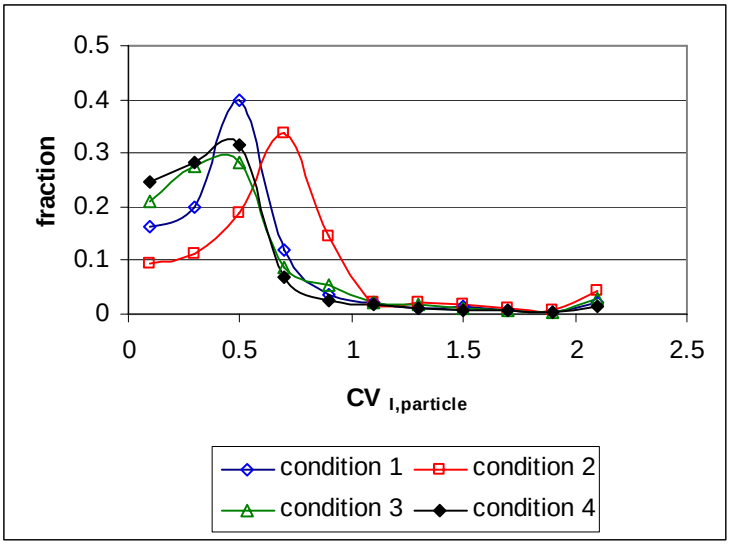

Figure 14-1: Coefficient of Variation plots about UV intensity for Reactor A

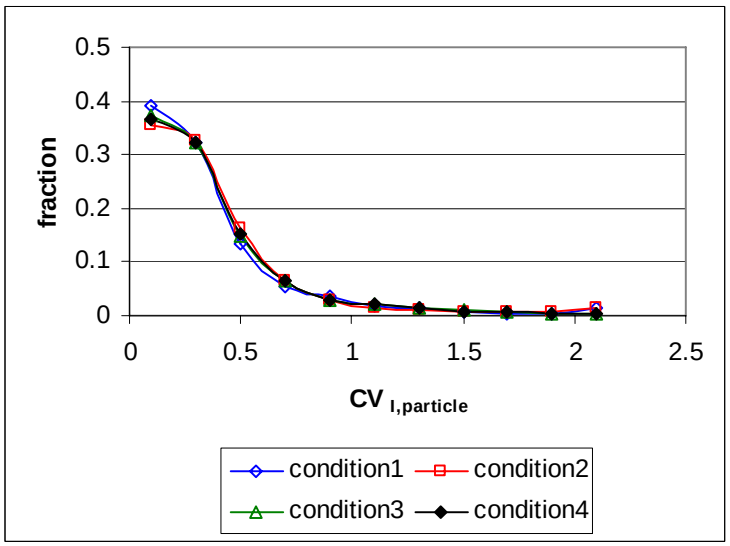

Figure 14-2: Coefficient of Variation plots about UV intensity for Reactor B

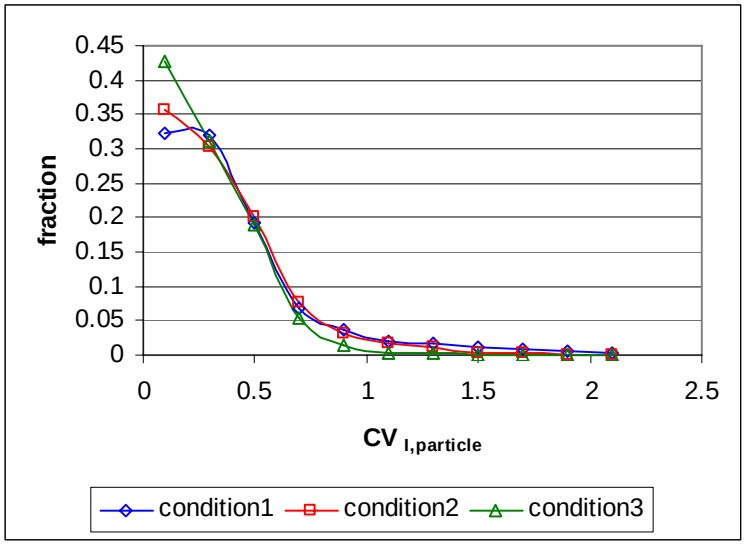

Figure 14-3: Coefficient of Variation plots about UV intensity for Reactor C

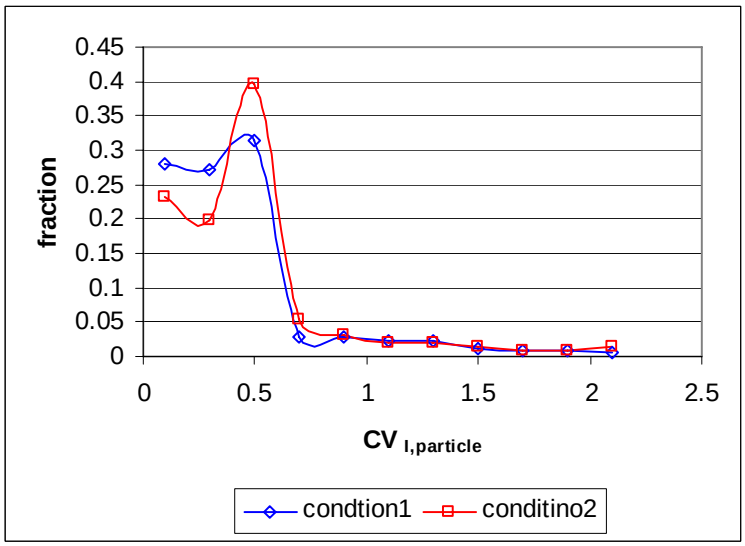

Figure 14-4: Coefficient of Variation plots about UV intensity for Reactor D

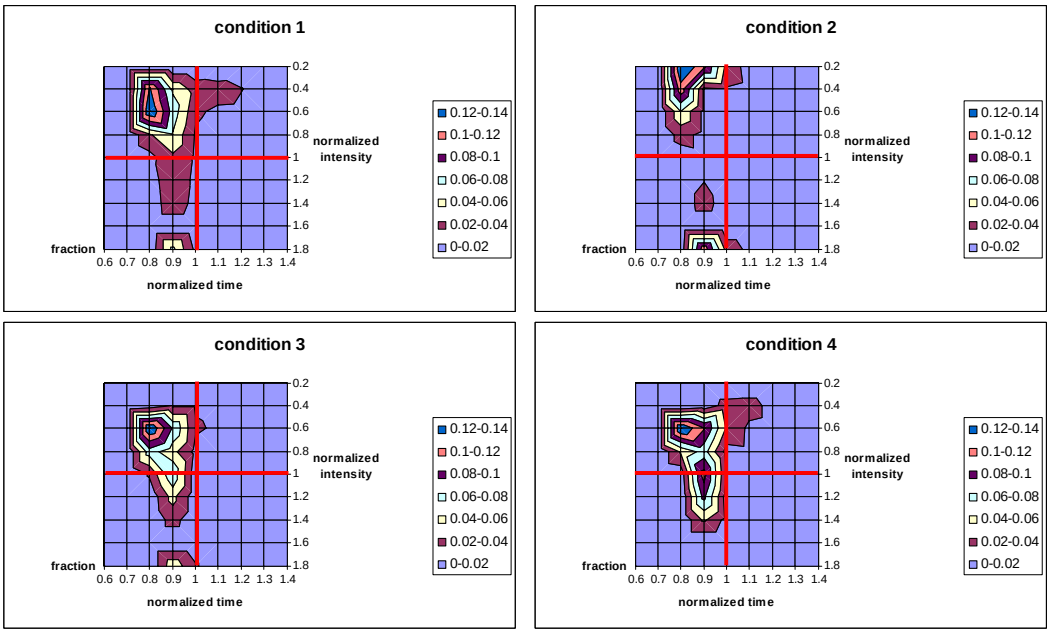

Figure 15-1: Contour plots for Reactor A under 4 different conditions, condition 1) avg. RT = 4.57sec, avg. I = 25.4 mW/cm2, condition 2) avg. RT = 4.29sec, avg. I = 18mW/cm2, condition 3) avg. RT = 3.65sec, avg. I = 25.51 mW/cm2, condition 4) avg. RT = 4.17sec, avg. I = 33.57 mW/cm2

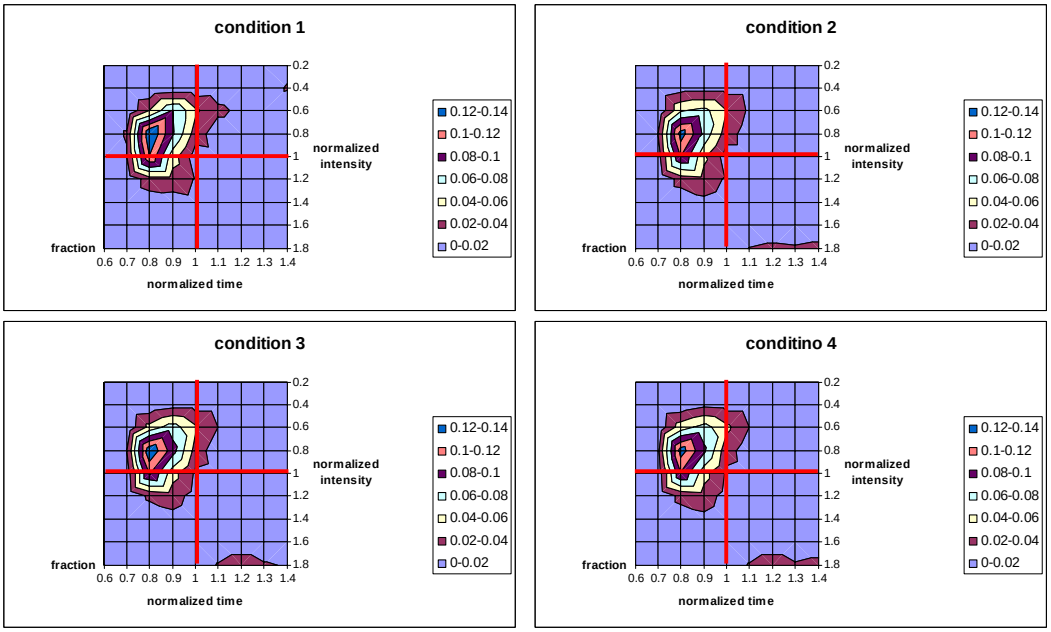

Figure 15-2: Contour plots for Reactor B under 4 different conditions, condition 1) avg. RT = 17.09sec, avg. I = 6.8 mW/cm2, condition 2) avg. RT = 6.15sec, avg. I = 8.62mW/cm2, condition 3) avg. RT = 4.33sec, avg. I = 14.82 mW/cm2, condition 4) avg. RT = 4.33sec, avg. I = 11.95 mW/cm2

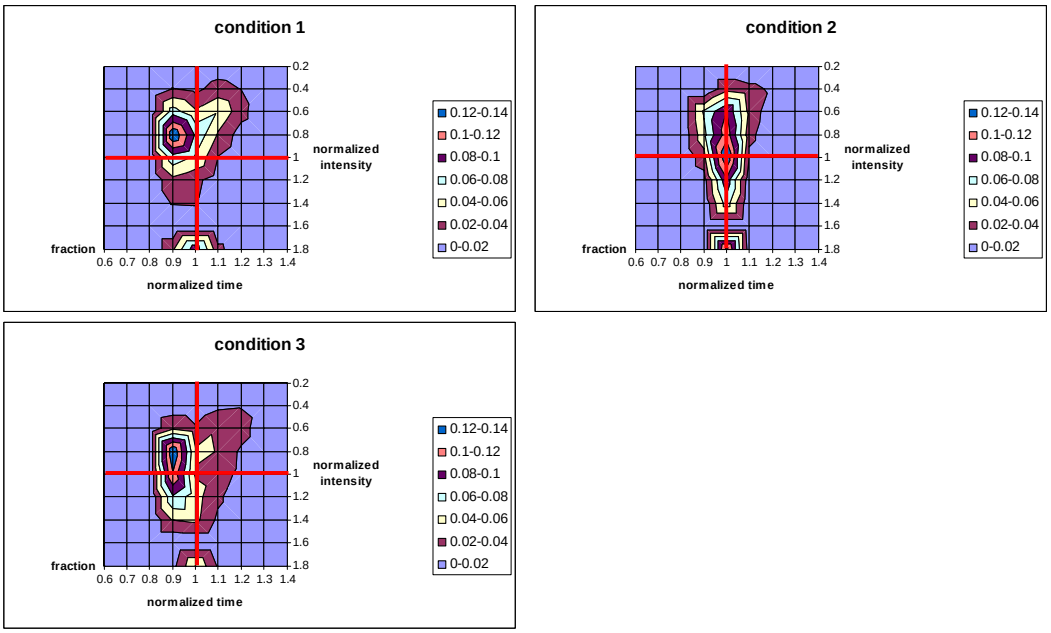

Figure 15-3: Contour plots for Reactor C under 3 different conditions, condition 1) avg. RT = 6.45sec, avg. I = 1.95 mW/cm2, condition 2) avg. RT = 6.43sec, avg. I = 4.88mW/cm2, condition 3) avg. RT = 11.48sec, avg. I = 6.1 mW/cm2

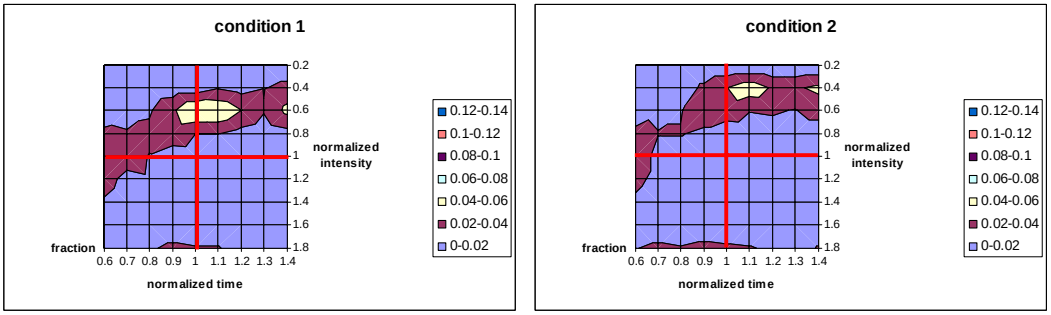

Figure 15-4: Contour plots for Reactor D under 2 different conditions, condition 1) avg. RT = 4.42sec, avg. I = 11.46 mW/cm2, condition 2) avg. RT = 2.33sec, avg. I = 9.46mW/cm2

a)

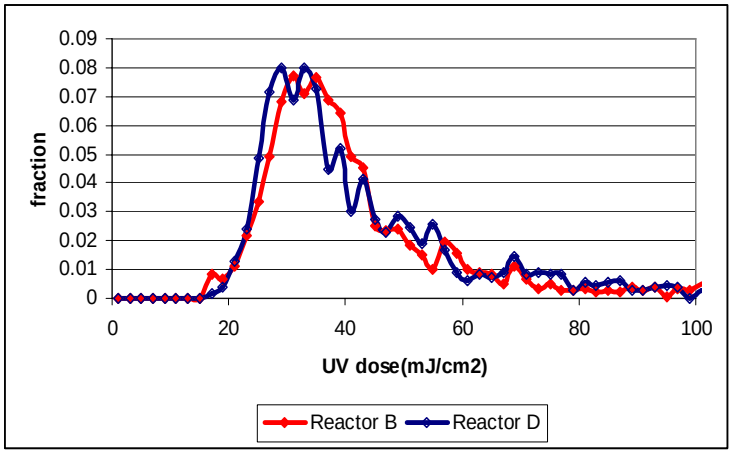

b)

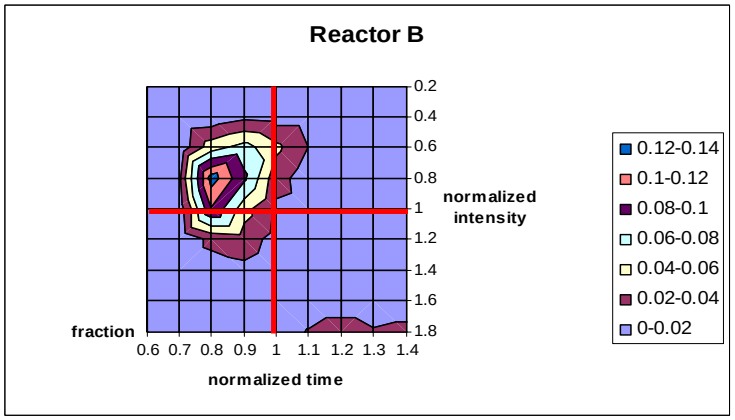

c)

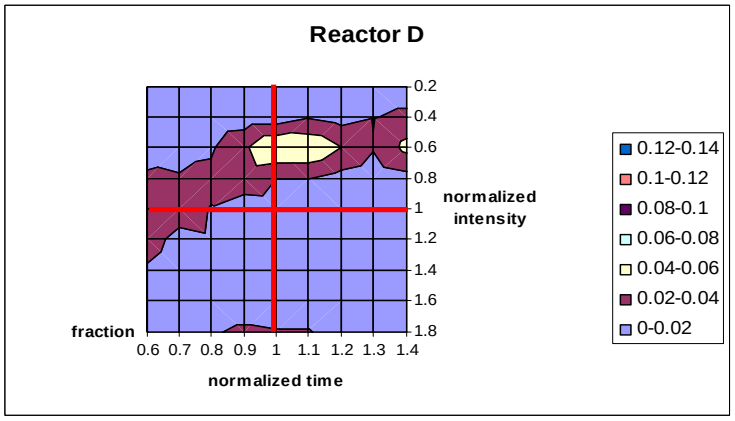

Figure 16: Comparing between reactor B and D based on UV dose distributions and contour plot: a) UV dose distributions for reactor B and Reactor D, b) contour plot for Reactor B in condition 4, c) contour plot for Reactor D in condition 1

a)

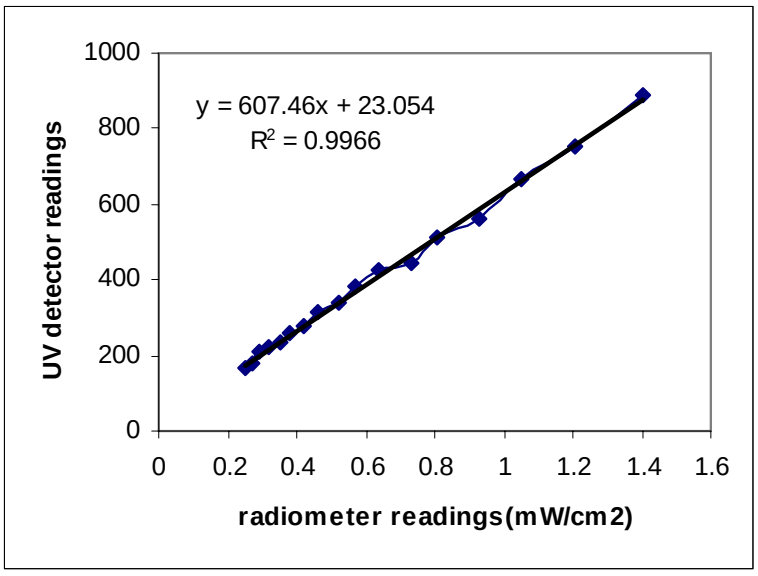

b)

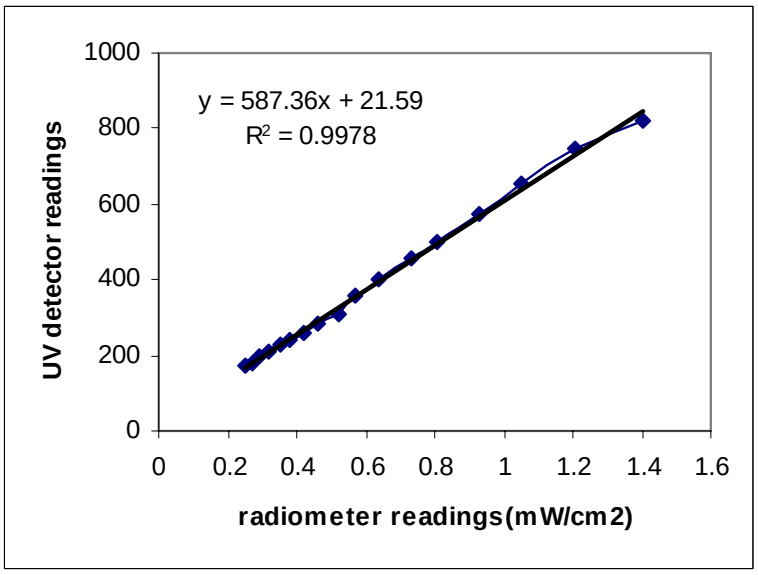

Figure 17-2: Calibration curves for both sensors: a) Sensor 1, b) Sensor 2

a)

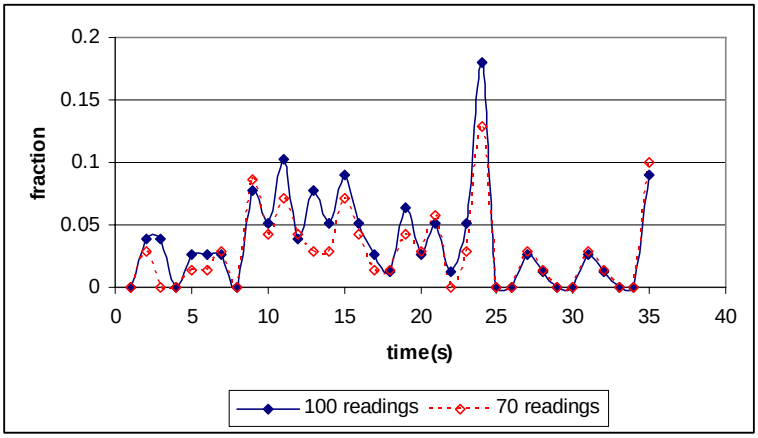

b)

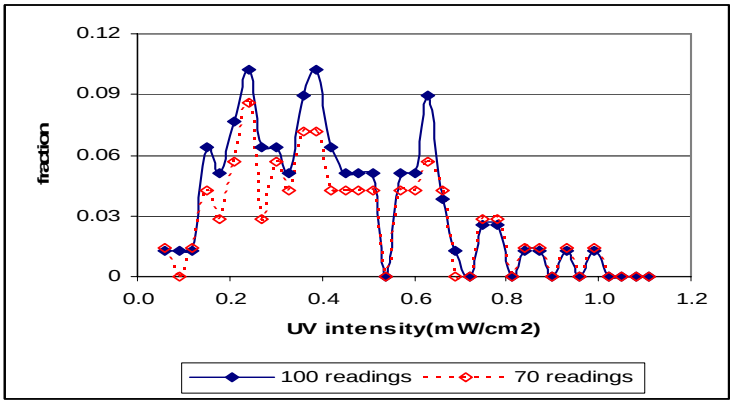

c)

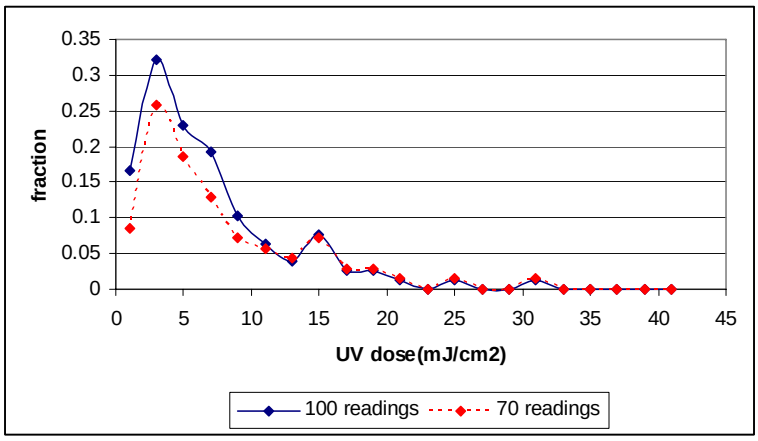

Figure 18: a) residence time distribution, b) UV intensity distribution, c) UV dose distributions obtained from results in pilot test

a)

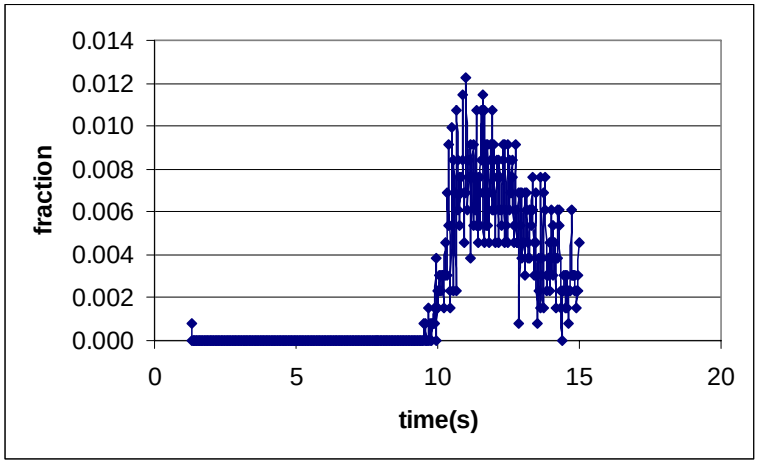

b)

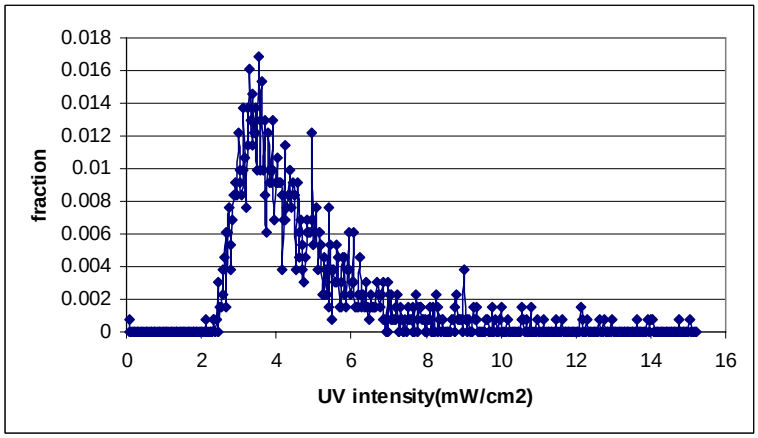

c)

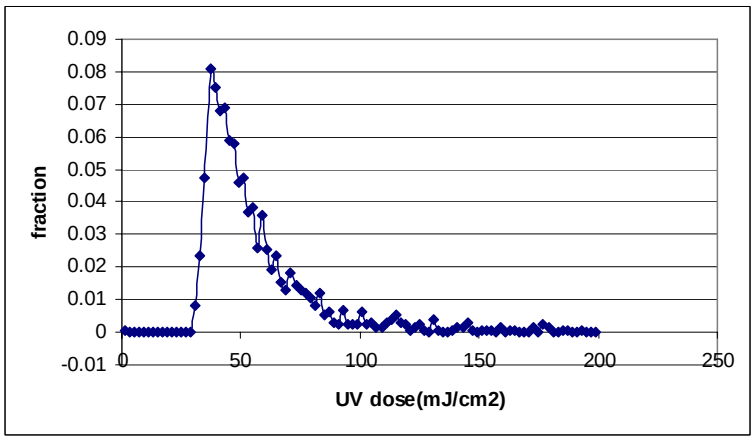

Figure 19: a) residence time distribution, b) UV intensity distribution, c) UV dose distributions obtained from results in modeling data

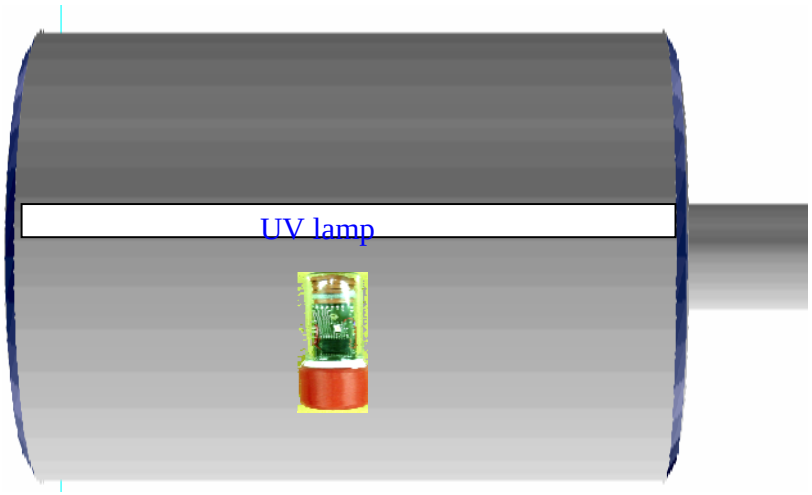

Figure 20: Lagrangian sensor movement in an upward stance configuration during traveling through the reactor